"Several birds with one stone" strategy of pH/thermoresponsive flame-retardant/photothermal bactericidal oil-absorbing material for recovering complex spilled oil

Ya Chen,[a] Jing Lin,[a,],* Gaber A. M. Mersal[b], *Jianliang Zuo,[a] Jialin Li,[a] Qiying Wang,[a] Yuhong Feng,[a] Jianwei Liu,[a] Zili Liu,[a,]* Bin Wang,[c] Ben Bin Xu,[d] Zhanhu Guo[e,]**

a. *School of Chemistry and Chemical Engineering, Guangzhou University, Guangzhou 510006, China*

b. *Department of Chemistry, College of Science, Taif University, P.O. Box 11099 Taif 21944, Saudi Arabia*

c. *College of Materials Science and Engineering, Taiyuan University of Science and Technology, Taiyuan, 030024, Shanxi, China*

d. *Department of Mechanical and Construction Engineering, Faculty of Engineering and Environment, Northumbria University, Newcastle upon Tyne, NE1 8ST, UK*

e. *Integrated Composites Laboratory (ICL), Department of Chemical & Biomolecular Engineering, University of Tennessee, Knoxville, TN 37996, USA*

*Corresponding authors.
E-mail addresses: linjin00112043@126.com or linjing@gzhu.edu.cn (J. Lin); zlliu@gzhu.edu.cn (Z. Liu) or zguo10@utk.edu or nanomaterials2000@gmail.com (Z. Guo)

Abstract

Although many material designs or strategic methods have been proposed for treating oil spills and oily wastewater, the complex oily state, dealing with the harsh operating conditions of oil–water separation (such as the recovery of viscous spilled crude oil, bacteria-containing oily wastewater, and removal of spilled oil under fire), and the autorecycling of oil and absorption materials remain a great challenge. This paper proposes an ingenious design strategy of "several birds with one stone" to prepare pH/thermoresponsive flame-retardant/photothermal bactericidal P-Fe_3O_4-polydopamine (PDA)@ melamine–formaldehyde (MF) foams. This design makes the foams remarkably effective in the recovery of spilled viscous crude oil as well as in the separation of bacteria-containing oily emulsions, particularly for instant fire extinguishing by magnetically controlled oil absorption as well as for fire alarms. The photothermal effect and pH response induce a change in the surface wettability of the foams, facilitating excellent autoadsorption/desorption of the spilled oil. The photothermal bactericidal activity and fouling resistance of the foam are beneficial to the separation of bacteria-containing oily wastewater. Outstanding flame-retardant properties and maneuverable magnetic control enable the foam to rapidly recover the spilled oil in a large range of fires, extinguish fires instantly, and facilitate early fire warning. The proposed strategy is expected to inspire further research on treating oil spills under complex conditions.

Keywords: oil-absorbing material; pH-responsive; thermoresponsive; photothermal; bactericidal; fire warning.

1. Introduction

Frequent accidental oil spills and the consequent formation of oily wastewater seriously endanger the ecological environment and human health as well as result in considerable economic loss and energy wastage [1-4]. Many methods have been developed to treat such oily wastewater; examples are chemical (e.g., flocculation and in situ combustion) [5-7], biological (e.g., microbial decomposition and repair) [8, 9], and physical (e.g., skimmers, gravity separation, and adsorption) methods [10-12]. Physical adsorption is the most straightforward and the least energy-consuming method [13-15]. A variety of adsorption materials, including sponge/foam [16-19], aerogel [20-24], and porous particles [25], are available. Among them, polyurethane (PU) foam, melamine–formaldehyde (MF) foam, and others have attracted considerable attention because of their high absorption rate, good mechanical durability, low cost, and facile design. For the selective absorption of spilled oil from water, considerable progress was made to modify the hydrophilic oil-absorbing foams to hydrophobic/oleophilic foams to impart high oil-absorbing capability and good water-repellency to the foam in the separation process [26-30].

However, the complex oily state or some harsh operating conditions of oil–water separation, low energy consumption for oil recovery, and the autorecycling of oil-absorbing materials remain great challenges [31, 32]. For example, the autoadsorption of crude oil on oil-absorbing foam is challenging at room temperature because of the crude oil's high viscosity ($> 10^3$ mPa s) [33-39]. In terms of the maneuverability of oil recovery, oil-absorbing materials can be blown away easily by sea breezes, making recovery difficult [40, 41]. There is a potential fire hazard in the recovery operation process of spilled oil because oil products are flammable [42, 43]. After the successful recovery of spilled oil from the ocean or oily wastewater, potentially harmful bacteria and

microorganisms can multiply in the water and even harm humans [44-47]. Therefore, this paper proposes a "several birds with one stone" design strategy of designing an oil-absorbing foam.

The photothermal method of reducing viscosity is a more promising method than the heating method to overcome the difficulty in oil absorption arising from the poor fluidity of the highly viscous crude oil. For example, Huang et al. developed a melamine sponge (m-CNT/PPy@MS) coated with superhydrophobic/oleophilic carbon nanotubes (CNTs) and polypyrrole (PPy) that can convert light and electricity into heat, remarkably reducing the viscosity of crude oil and allowing the sponge to absorb the spilled oil quickly [48]. Yang et al. used polydopamine as a photothermal component and introduced a polydimethylsiloxane (PDMS) layer into a melamine–formaldehyde sponge to achieve a hydrophobic/oleophilic effect, which can also improve the adsorption performance of high-viscosity crude oil [49]. However, the desorption of oil from most oil-absorbing materials needs to be addressed using energy-consuming treatment methods, such as mechanical extrusion [50, 51], combustion [52, 53], distillation, and centrifugation [54, 55]. Some of these methods can destroy the structure of the adsorbent materials or consume high energy, which may cause secondary pollution to the environment. Methods to deal with the problem of fire during the recovery process of oil spills are rarely reported; in this regard, a flame-retardant oil-absorbing foam is an ideal choice. For instance, Feng et al. developed a nonflammable and magnetic MF foam decorated with a PDMS brush for multitasking and achieving highly efficient oil–water separation [56]; Jiang et al. reported a magnetic and flame-retardant superhydrophobic MF foam for solar-assisted high-viscosity oil–water separation [57].

Few studies have examined the bacteria that may persist in purified water after the successful recovery of spilled oil from the ocean or oily wastewater. The bactericidal treatment of such water was only reported in the membrane separation of oil–water wastewater [58-62]. The following

issues still need to be studied pertaining to oil-spill recovery; efficient and energy-saving desorption of adsorbed oil using foam, autorecycling the oil-adsorbing foam, managing the fire risk, and tackling bacterial contamination.

This paper proposes a design strategy of pH/thermoresponsive flame-retardant/photothermal bactericidal P-Fe_3O_4-PDA@MF oil-absorbing material, which was prepared by a five-step process **(Fig. 1a)**, to achieve the efficient autoadsorption/desorption of spilled oil, bacterial contamination treatment, and fire management. In particular, the designed porous MF foam has deposited PDA/Fe_3O_4 composite nanoparticles (NPs) that enable the foam to be heated or cooled under sunlight irradiation or being removed. The thermoresponsive polymer molecules incorporated on the MF foam can migrate and change its surface wettability from hydrophilicity/oleophilicity to hydrophobicity/oleophilicity, thereby reducing the viscosity of the crude oil for improving adsorption capacity. Meanwhile, adjusting the pH-responsive polymer molecules incorporated into the MF foam can enhance the hydrophilicity/oleophobicity as well as improve the autodesorption properties of the conventional crude oil without an extrinsic energy input. Furthermore, the bactericidal activity of the photothermal effect can kill the bacteria in the oil-containing wastewater, and the oil/bacteria can be separated from the emulsion. This study explores the fire-extinguishing effect and fire-warning performance of MF foam for urgently treating the spilled oil in the event of a fire (**Fig. 1b**).

2. Materials and methods

2.1 Materials

Commercial melamine–formaldehyde (MF) foams were purchased from the local market. Dopamine hydrochloride and copper (II) sulfate pentahydrate ($CuSO_4 \cdot 5H_2O$, ≥99.0%) were obtained from Shanghai Macklin Biochemical Co., Ltd. Tris(hydroxymethyl)aminomethane was

purchased from Sigma–Aldrich. Hydrogen peroxide (H_2O_2, 30%) was acquired from Guangzhou Chemical Reagent Factory, and iron (III) chloride hexahydrate ($FeCl_3 \cdot 6H_2O$, ≥99.0%) was supplied by Sinopharm Chemical Reagent Co., Ltd. Ethylene glycol ($C_2H_6O_2$, 98%), sodium acetate (CH_3COONa, ≥99.0%), Sudan III, and vinyltrimethoxysilane (VTMS, >98%) were obtained from Shanghai Aladdin Biochemical Technology Co., Ltd. *N*-isopropylacrylamide (NIPAAm, 98%), *N,N′*-methylenebisacrylamide (MBA, 99%), 2-(dimethylamino)ethyl methacrylate (DMAEMA, 99%), ammonium persulfate (APS, 98.5%), hexadecyltrimethoxysilane (HDTMS, ≥85%), Tween 80, and various oily substances (tetrachloromethane, 1,2-dichloroethane, toluene, petroleum ether, acetone, *n*-hexane, and cyclohexane) were acquired from Shanghai Macklin Biochemical Co., Ltd. Crude oil was provided by PetroChina. *Escherichia coli* [CMCC(B) 44102] (*E. coli*) and *Staphylococcus aureus* [CMCC(B) 26003] (*S. aureus*) were procured from Shanghai Luwei Microbial Sci. & Tech. Co., Ltd. Phosphate-buffered saline (PBS), nutrient agar (NA), and nutrient broth were purchased from Sigma–Aldrich. The LIVE/DEAD BacLight bacterial viability kit was supplied by Invitrogen (Carlsbad, CA, USA).

2.2 Preparation of Fe_3O_4 NPs

Fe_3O_4 NPs were prepared using a hydrothermal method. Typically, $FeCl_3 \cdot 6H_2O$ (1.35 g) and $CH_3COONa \cdot 3H_2O$ (3.6 g) were dissolved in ethylene glycol (40 mL), stirred at room temperature for 10 min, transferred to a Teflon-lined autoclave, and placed in an oven at 200°C for a heating reaction for 8 h. After natural cooling, a Fe_3O_4 NPs solution was obtained. Solid–liquid separation was performed using a magnet, and the solid was washed thrice with anhydrous ethanol and deionized water. Finally, Fe_3O_4 NPs powder was obtained using a freeze-drying machine.

2.3 Preparation of Fe_3O_4-PDA@MF foam

Fe_3O_4-PDA@MF foam was prepared via multistep impregnation deposition. Typically, MF foams were cut into small cubes of 2 × 2 × 1 cm^3 as a matrix. A small amount of impurities was removed by repeated ultrasonic cleaning with ethanol and deionized water and subsequent drying in an oven at 80°C. Dopamine hydrochloride (0.1 g, 2 mg mL^{-1}), $CuSO_4$ (0.0625 g, 5 mmol L^{-1}), and H_2O_2 (0.1 mL, 19.6 mmol L^{-1}) were dissolved in a Tris-buffer solution (pH = 8.5, 0.2 mol L^{-1}) to form a mixed solution [63]. The foam was immersed in a mixed solution for 1 h, and PDA was modified on the foam to obtain PDA@MF. The PDA that was not deposited on the foam was washed off thrice with deionized water, and then the foam was dried in an oven at 80°C. PDA@MF foam was then immersed in 10 mL Fe_3O_4 aqueous dispersion (3 mg mL^{-1}) for 20 min and dried for 2 h in an oven at 80°C. Following the above steps, the layers of PDA and Fe_3O_4 composite NPs were deposited thrice to obtain Fe_3O_4-PDA@MF foam.

2.4 Preparation of P-Fe_3O_4-PDA@MF foam

P-Fe_3O_4-PDA@MF foam was prepared via in situ free-radical polymerization. Typically, VTMS (300 μL) was dissolved in 15 mL of an ethanol solution containing 20% deionized water. A certain amount of ammonia (25%) was added to adjust the pH to 10, and Fe_3O_4-PDA@MF foam (2 × 2 × 1 cm^3) was immersed in the solution for silanization for 30 min. After washing with deionized water and drying at 100°C for 1 h in an oven, VTMS-Fe_3O_4-PDA@MF foam was obtained. VTMS-Fe_3O_4-PDA@MF, NIPAAm (0.7544 g), DMAEMA (0.2620 g), and MBA (0.0203 g, 2.5 wt% of the total monomer) were added to deionized water (solid content is 4 wt%) and stirred evenly to produce the initiator solution of APS (0.156 g, 1.5 wt% of the total monomer, 2 mg mL^{-1}), which was dropped into the above mixture. The formed polymer was modified on foam via in situ free-radical polymerization at 80°C for 6 h. The polymer-modified NIPAAm-*co*-

DMAEMA-co-MBA foam was immersed in deionized water thrice to remove unreacted monomers and residual small molecules as well as freeze-dried to remove water. Finally, HDTMS (50 μL) was dissolved in a 15 mL ethanol solution containing 20% deionized water. A certain amount of ammonia (25%) was added to adjust the pH to 10, and the modified foam was immersed in the HDTMS solution for 30 min for silanization. After rinsing with deionized water, the foam was placed in an oven at 100°C for drying for 1 h to obtain polymer and silane modified P-Fe_3O_4-PDA@MF foam.

2.5 Characterizations and measurement

The micromorphology of the foam was observed using a field emission scanning electron microscope (SEM, JSM-7001F, JEOL, Japan), and the pore structure of the foam was characterized using a high-performance automatic mercury press (AutoPore V 9600, Micromeritics, USA). The chemical functional groups on the foam surface were examined by attenuated full reflection–Fourier transform infrared spectroscopy (ATR–FTIR, TENSOR II, Bruker, Germany). The elemental components on the foam surface were tested using X-ray photoelectron spectroscopy (XPS, K-Alpha+, Thermo Fisher Scientific, USA). The elemental content on the foam surface was analyzed using energy dispersive spectroscopy (EDS, Model Inca400, Oxford Instruments, UK). Fe_3O_4 NPs and their crystal structures on the foam were characterized using X-ray diffraction (XRD, Ultima VI, Rigaku, Japan) analysis. The saturation magnetizations of Fe_3O_4 NPs and their modified foam were measured using vibration sample magnetometry (Lake Shore 7404, USA) within the magnetic field range of –10000 to 10000 Oe. The temperature sensitivity of the synthesized responsive polymer was determined using differential scanning calorimetry (DSC,

DSC8000, PerkinElmer, USA) to characterize its lower critical solution temperature (LCST). The water contact angle (WCA), oil contact angle (OCA), and underwater oil contact angle (UWOCA) on the foam surface were measured using a contact angle meter (OCA40 Micro, DataPhysics, Germany).

The surface and interfacial tensions of the liquid and the adhesion force of the foam surface were measured using a highly sensitive micromechanical balance system (K100, Kruss, Germany). The droplet sizes of the feed and filtrate of the bacteria-containing oil/water emulsion were measured using a nanoparticle size meter (Malvern ZS90, UK) to evaluate the effects of oil separation. Fluorescence staining was used to evaluate the number distribution of bacteria in the feed and filtrate. The dead and alive states of the bacteria after dyeing were studied by fluorescence microscopy (Olympus BX51, Japan), and the excitation and emission wavelengths were 440–480 nm and 515–540 nm, respectively. The change in the foam temperature was detected using an infrared thermal imager (FLIR E54, USA). The thermal stability of the foam was analyzed using a thermogravimetric analysis (TGA, TGA4000, PerkinElmer, USA).

2.6 Oil absorption and desorption capacities of P-Fe_3O_4-PDA@MF foam

An oil adsorption experiment was performed. P-Fe_3O_4-PDA@MF foam was illuminated under a xenon lamp that provided simulated sunlight with a light intensity of 1.0 kW m^{-2} for 5 min. The intensity was measured using a light intensity meter by adjusting the light power and irradiation distance between the samples and xenon lamp; it was subsequently immersed in different light oily substances (i.e., tetrachloromethane, 1,2-dichloroethane, toluene, petroleum ether, acetone, and cyclohexane) and viscous oils (i.e., silicone oil, pump oil, and crude oil). The P-Fe_3O_4-PDA@MF

foam absorbed the oils for 2 min until adsorption saturation was reached, and the oil absorption capacity of different oil products was tested. The saturation oil absorption capacity of the foam was calculated using Eq. (1) [64]:

$$k_a = \left(\frac{m_1}{m_0} - 1\right) \times 100\% \quad (1)$$

where m_0 *and* m_1 represent the quality of P-Fe_3O_4-PDA@MF foam before and after oil absorption, respectively, and k_a is the saturation oil absorption capacity.

An oil desorption experiment was performed. In this experiment, after P-Fe_3O_4-PDA@MF foam absorbed light oil (cyclohexane) and heavy oil (1,2-dichloroethane), it was transferred to water (with pH = 1) and soaked for a period of time to release the absorbed oil. After the oil was released, the oil above or below the water was recovered using a separation device and weighed. The desorption rate of oil was calculated according to Eq. (2):

$$k_d = \left(\frac{m_2}{m_1 - m_0}\right) \times 100\% \quad (2)$$

where $m_0$and m_1 represent the quality of P-Fe_3O_4-PDA@MF foam before and after oil absorption, respectively; m_2 represents the quality of the desorbed oil; and k_d represents the desorption rate of oil. After desorption, P-Fe_3O_4-PDA@MF foam was washed completely with deionized water and freeze-dried. The above steps were repeated 10 times to test the recyclability of oil desorption by the foam.

2.7 Separation of oil–in–water emulsion containing bacteria

A stable oil–in–water emulsion was produced by adding Tween 80 (0.1 g) to deionized water (99 mL). Subsequently, *n*-hexane (1 mL) was added dropwise to the aqueous solution at a ratio of 1:99 (v/v), and this was followed by emulsifying with magnetic stirring for 2 h. To configure an

emulsion containing bacteria, the emulsion (5 mL) containing 10^7 CFU mL^{-1} bacterial suspension (*S. aureus* or *E. coli*) as the feed liquid was poured into the separation funnel device with P-Fe_3O_4-PDA@MF foam for filtration. The filtrate (100 μL) was then coated on a petri dish containing NA and cultured at 37°C for 24 h. The number of collected bacteria was counted and compared with the feed emulsion. The bacterial separation rate was calculated using Eq. (3) [65]:

$$Bacterial\ separation\ rate(\%) = \left(\frac{CFU_{feed}mL^{-1} - CFU_{filtrate}mL^{-1}}{CFU_{feed}mL^{-1}}\right) \times 100\% \quad (3)$$

where $CFU_{feed}\ mL^{-1}$ and $CFU_{filtrate}\ mL^{-1}$ represent the average number of bacteria in the feed emulsion and filtrate, respectively.

2.8 Photothermal antibacterial property of P-Fe_3O_4-PDA@MF foam

The separation device was placed under a xenon lamp after filtering the oil–in–water emulsion containing bacteria and was irradiated with the lamp that provided simulated sunlight with a light intensity of 3.0 kW m^{-2} for 90 min to kill the bacteria on the surface of P-Fe_3O_4-PDA@MF foam. During this process, the change in the foam temperature was monitored using an infrared thermal imager. The foam was then immersed in a PBS solution (10 mL) and oscillated for 30 min to shake the bacteria on the surface into the PBS solution. After dilution by a certain multiple with sterile water, the bacterial solution (100 μL) was taken and coated on a petri dish containing NA and cultured at 37°C for 24 h. The number of bacteria was counted by multiplying the dilution factor. Compared with the original bacterial emulsion (as a control), the percentage decrease in the bacterial colonies was taken as the average of two duplicate tests. The antibacterial rate was calculated using Eq. (4):

$$Antibacterial\ rate(\%) = \left(\frac{CFU_{control}mL^{-1} - CFU_{sample}mL^{-1}}{CFU_{sample}mL^{-1}}\right) \times 100\% \quad (4)$$

where $CFU_{control}\ mL^{-1}$ and $CFU_{sample}\ mL^{-1}$ are the average number of bacteria on the control foam sample without illumination and on the foam sample after illumination, respectively.

3. Results and discussion

3.1 Preparation and characterization of P-Fe₃O₄-PDA@MF foam

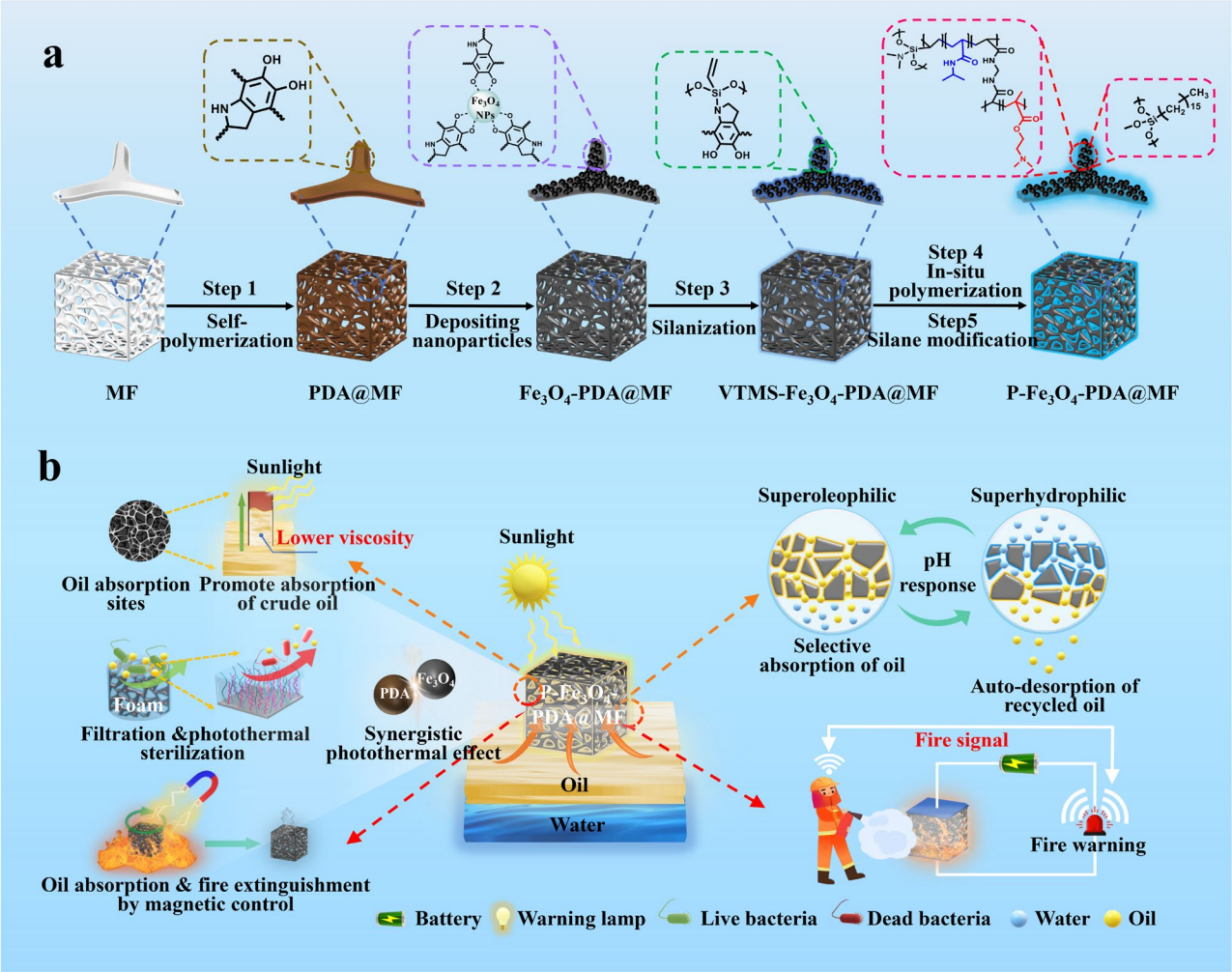

Fig. 1. a) Schematic diagram of the preparation process of multiresponse oil-absorbing foam; and b) application of P-Fe₃O₄-PDA@MF foam in complex oil spill treatment.

Fig. 1a presents a schematic of the five-step preparation process of the multiresponsive oil-absorbing foam. The surface morphology of the foam at different preparation stages was investigated using scanning electron microscopy (SEM). The pristine MF foam exhibited a three-

dimensional porous network structure and a smooth surface, with a porosity of 95.9% and an average aperture of roughly 223.6 μm (**Fig. 2a and S1**). The presence of a large number of micropores in the foam is critical in determining the oil absorption rate and oil adsorption capacity. After dopamine modification (Step 1), the MF foam skeleton was covered with a layer of PDA NPs (**Fig. 2b**). The PDA@MF foam was then immersed in a magnetic Fe_3O_4 NPs dispersion (3 mg mL^{-1}) with a mean particle size of approximately 1,076 nm (**Fig. S2**), and Fe_3O_4 was anchored successfully at the metal chelation site provided by PDA. After the chelation reaction (Step 2), a rough foam pore surface of the micro–nanoscale was formed (**Fig. 2c**). Subsequently, further silanization by VTMS was performed to introduce double-bond polymerizable sites (Step 3). A poly (NIPAAm-co-DMAEMA) copolymer layer composed of NIPAAm and DMAEMA was coated uniformly on the foam skeleton after in situ free-radical polymerizations (Step 4) (**Fig. 2d**) and then, the foam was silanized further using HDTMS to impart good oleophilicity (Step 5).

Fig. 2e shows the X-ray diffraction (XRD) results of the self-made Fe_3O_4 and its modified MF foam. The characteristic XRD peaks of Fe_3O_4 appear at $2\theta = 30.17°$, 35.53°, 43.12°, 53.56°, 56.99°, and 62.54°, corresponding to (220), (311), (400), (422), (511), and (440) crystal planes of cubic Fe_3O_4 (JCPDS card no. 19-0629), respectively, and these peaks confirm the successful synthesis of Fe_3O_4 NPs. For MF and PDA@MF foam, there is no prominent characteristic XRD peak. However, both Fe_3O_4-PDA@MF and P-Fe_3O_4-PDA@MF foam, which were modified by Fe_3O_4, PDA, and polymers, showed the typical characteristic XRD peaks of Fe_3O_4 NPs. This finding proves the modification of magnetic Fe_3O_4 on the foam. The porosity of the modified P-Fe_3O_4-

PDA@MF foam is high at 92.5%, and the average pore size is approximately 139.0 μm, which is smaller than that of the foam before modification but retains high porosity (**Fig. S1**).

The organic components of the polymers on the sponge surface were characterized using ATR–FTIR (**Fig. 2f**). The MF foam exhibits typical characteristic peaks at 3334 cm^{-1} (N–H stretching vibration), 1544 cm^{-1} (C=N stretching vibration), and 808 cm^{-1} (triazine ring bending vibration). The Fe_3O_4-PDA@MF spectrum shows typical characteristic peaks at 1586 cm^{-1} (N–H shear vibration), 1517 cm^{-1} (aromatic ring C=C skeleton vibration), and 1281 cm^{-1} (C–O bending vibration), indicating that PDA was deposited on the MF foam. The Fe–O typical characteristic peak at 548 cm^{-1} shows that Fe_3O_4 was chelated on MF foam through PDA. Unlike the Fe_3O_4-PDA@MF spectrum, the spectrum of VTMS-Fe_3O_4-PDA@MF exhibited asymmetric stretching vibration and symmetric stretching vibration peaks of C=C–H at 3061 cm^{-1} and 3026 cm^{-1}, respectively; characteristic absorption peaks at 1600 and 1408 cm^{-1} ($CH=CH_2$ shear vibration); absorption peaks of 1101 cm^{-1} (Si–O–Si stretching vibration); and characteristic absorption peaks at 754 cm^{-1} (Si–C stretching vibration). This suggests that Fe_3O_4-PDA@MF has been silanized and contains double bonds.

After polymer incorporation and silane modification in P-Fe_3O_4-PDA@MF, the spectrum exhibited typical characteristic peaks of the DMAEMA segments, such as 1719 cm^{-1} (C=O stretching vibration) and 1151 cm^{-1} (C–N stretching vibration), and the absorption peaks of amide groups from MBA and NIPAAm segments, such as the peaks at 1636 cm^{-1} (C=O stretching vibration), 1546 cm^{-1} (N–H bending vibration), 1459, and 1387 cm^{-1} (the stretching vibration absorption peaks of $–CH(CH_3)_2$). Meanwhile, the characteristic absorption peak at 1600 cm^{-1}

(C=C) disappeared, suggesting that the introduced double bond reacted completely with the NIPAAm and DMAEMA monomers. The copolymer was grafted successfully to VTMS-Fe_3O_4-PDA@MF. P-Fe_3O_4-PDA@MF was finally obtained after silanization by HDTMS, as indicated by the absorption peaks corresponding to the long alkyl chain; for example, the absorption peaks at 2971 cm^{-1} ($–CH_3$) and 2921 cm^{-1} ($–CH_2–$).

EDS results revealed the elemental distribution of P-Fe_3O_4-PDA@MF (**Fig. 2g**), confirming that C, N, O, Si, and Fe were distributed uniformly on the foam skeleton, with atomic ratios of 72.48%, 10.73%, 15.27%, 0.20%, and 1.31%, respectively. The uniform distribution of iron suggests that Fe_3O_4 NPs were distributed uniformly on the foam. The surface chemical bonds of P-Fe_3O_4-PDA@MF were analyzed further using XPS (**Fig. 2h**), and the main elements were detected: C 1s (284.2 eV), N 1s (398.4 eV), O 1s (530.6 eV), and Si 2p (101.1 eV). The C 1s spectrum showed some functional groups, such as C–C (284.8 eV), C–O/C–N (286.2 eV), C=O (287.3 eV), and O–C=O (288.5 eV), which originated from PDA, PolyNIPAAm (PNIPAAm) and PolyDMAEMA (PDMAEMA) chains covering the foam surface. The C=O (531.2 eV), Si–O (532.8 eV), Si–C (102.1 eV), and Si–O–Si (103.5 eV) functional groups in the O 1s and Si 2p spectra were derived from the siloxane molecules grafted on the foam surface.

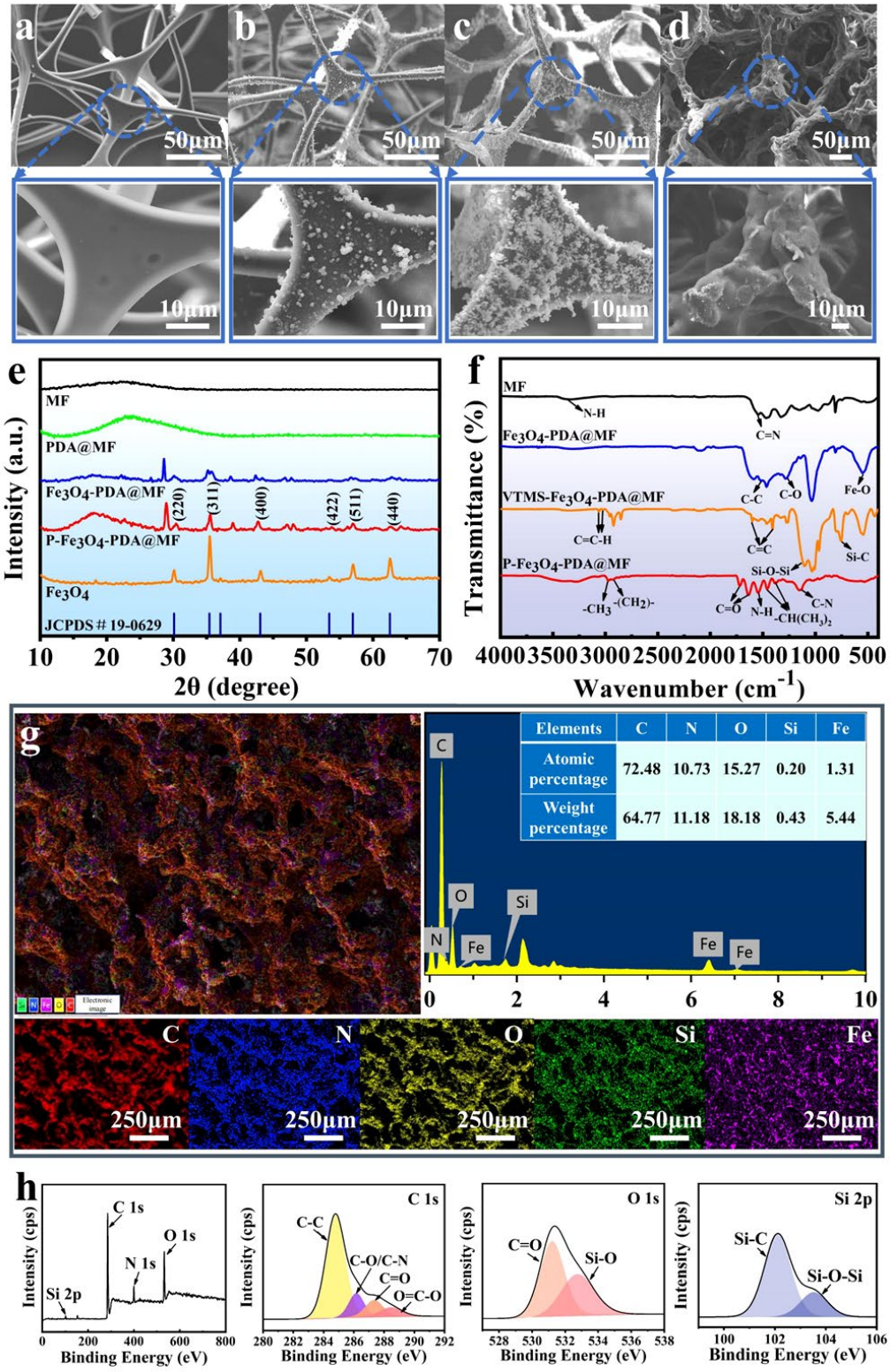

Fig. 2. SEM images of a) MF, b) PDA@MF, c) Fe_3O_4-PDA@MF, and d) P-Fe_3O_4-PDA@MF; e) ATR–FTIR and f) XRD of foams at different preparation stages; g) SEM–EDS mapping distribution of various elements on P-Fe_3O_4-PDA@MF. h) XPS spectra of P-Fe_3O_4-PDA@MF.

3.2 Oil absorption performance of P-Fe_3O_4-PDA@MF foam

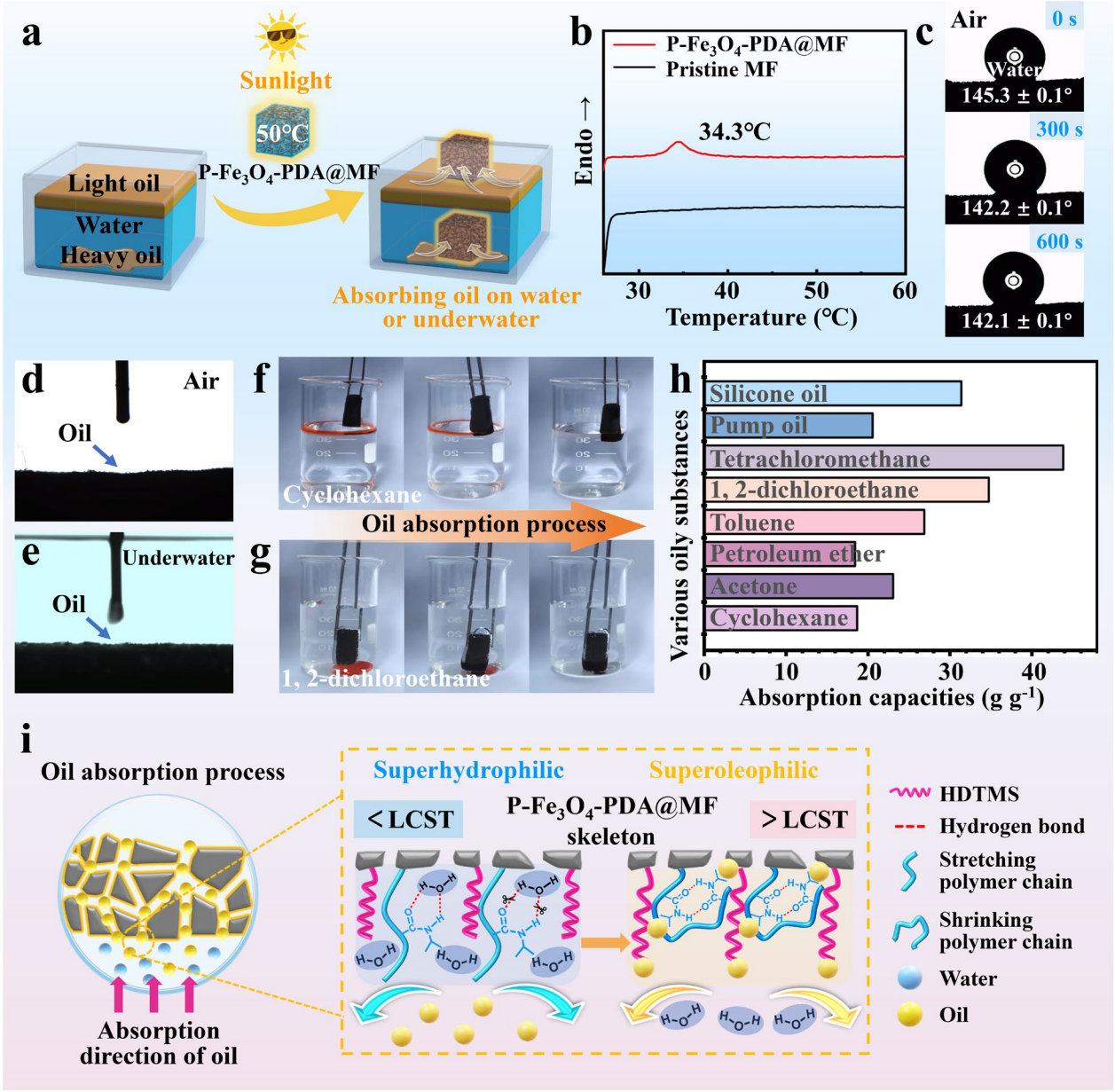

Fig. 3. a) Schematic diagram of the absorption process of oil on water and underwater before and after the thermoresponse of P-Fe_3O_4-PDA@MF. b) Differential scanning calorimetry (DSC) of P-Fe_3O_4-PDA@MF. c) Water contact angles (WCAs) of P-Fe_3O_4-PDA@MF at 50 °C. d) Oil contact angles (OCAs) on water and e) underwater oil contact angles (UWOCAs) of P-Fe_3O_4-PDA@MF. P-Fe_3O_4-PDA@MF adsorption photos of f) light oil (cyclohexane) and g) heavy oil (1, 2-dichloroethane) at 50 °C. h) Oil absorption capacities of various oily substances. i) Mechanism diagram of the thermoresponsive oil absorption process of P-Fe_3O_4-PDA@MF.

The introduction of a sufficient number of HDTMS alkyl chain molecules can impart superoleophilic/superhydrophobic properties as well as strong oil absorption capacity and hydrophobicity to porous materials; these properties are beneficial for the absorption of light oil in air and heavy oil underwater. However, this general method highlights the problems of easy oil absorption but difficult automatic oil desorption. Only mechanical extrusion, combustion, distillation, and other energy-consuming methods can be used to recover oil and achieve foam recycling. Additionally, some viscous oils remain in the porous materials, and the adsorption capacity often decreases after several oil-absorption cycles (**Fig. S3**). Hence, excellent recycling of the oil-absorbing materials cannot be achieved. Therefore, to achieve better desorption, a thermosensitive polymer PNIPAAm (whose LCST is approximately 32°C) [66] was introduced on the foam surface and in its pores, and the foam was further modified with Fe_3O_4 and PDA composite nanoparticles by the photothermal effect to form a responsive P-Fe_3O_4-PDA@MF foam.

When the foam is placed under simulated sunlight (i.e., the xenon lamp with an illumination intensity of 1.0 kW m^{-2}) and irradiated for 5 min, the temperature of the foam increases by a photothermal effect. The change in temperature alters the surface wettability of the foam (**Fig. 3a**). To this end, the instantaneous WCA of P-Fe_3O_4-PDA@MF foam in the air at different temperatures was explored. The WCA gradually increases with increasing temperature (132.2 ± 0.2° for 25°C and 145.3 ± 0.1° for 50°C) (**Fig. S4**). This is because the configuration of the functional groups of the thermosensitive polymer on the foam changes when the temperature of the foam becomes higher than the LCST of P-Fe_3O_4-PDA@MF, as shown in **Fig. 3b** (while the pristine MF foam does not exhibit any heat absorption peaks, the heat absorption peak of P-Fe_3O_4-PDA@MF foam

appears at 34.3°C), resulting in a change in the surface wettability to the extent that the foam exhibits persistent hydrophobicity exceeding 600 s at 50°C (**Fig. 3c**). These results suggest that P-Fe_3O_4-PDA@MF foam can maintain certain hydrophobicity by controlling the temperature at a value greater than that of the LCST. Moreover, air is trapped around the foam, forming an air/water/solid interface that reduces the contact area between the solid surface and water, preventing water infiltration when the foam absorbs the oil.

Meanwhile, the P-Fe_3O_4-PDA@MF foam exhibits both oleophilicity in air (OCA = 0°) and underwater (UWOCA = 0°) (**Fig. 3d and e**), ensuring that both light oil (cyclohexane) and heavy oil underwater (1,2-dichloroethane is absorbed rapidly by foam within 5 s) penetrate the foam rapidly because of capillary force (**Fig. 3f and g, Video S1**), occupy the internal space of the foam, and inhibit the infiltration of water. Furthermore, the oil absorption capacity of the foam was investigated to determine whether the P-Fe_3O_4-PDA@MF foam per unit mass has a high adsorption capacity for various oily substances. The results revealed absorption capacities of 31.40, 20.55, 43.83, 34.74, 23.07, and 18.67 g g^{-1} for silicone oil, pump oil, tetrachloromethane, 1,2-dichloroethane, toluene, and cyclohexane, respectively, suggesting that the foam is an excellent material for oil/water mixture separation (**Fig. 3h**).

Finally, the oil absorption process was examined by observing the conformation changes in thermosensitive molecules on the foam surface, as shown in **Fig. 3i**. The thermosensitive characteristics originate mainly from hydrophilic and hydrophobic equilibrium effects, and thermosensitive conformation changes can be analyzed using Eq. (5)[67]:

$$\Delta G = \Delta H - T\Delta S \quad (5)$$

where ΔG, ΔH, and ΔS represent the mixed Gibbs free energy, cosoluble enthalpy, and cosoluble entropy of thermosensitive polymers and water molecules, respectively; and T is the system temperature. ΔH is related to the intermolecular interaction forces in the system and ΔS depends on the order of the system. Thermodynamically, when ambient temperature is lower than the LCST, intermolecular hydrogen bonds (IHBs) are formed between water molecules and amide groups (HN–C=O) in the PNIPAAm molecular chain of the polymer, resulting in a low degree of freedom; thus, the −TΔS of the system is positive, and the formation of a hydrogen bond is exothermic (ΔH < 0), so ΔG becomes less than 0 at low temperatures. When the temperature of the thermosensitive polymer is higher than the LCST, the stability of IHBs between water molecules and amide groups (HN–C=O) decreases, leading to the breakage of the hydrogen bonds and resulting in a less exothermic effect and a low ΔH. When the temperature increases, −TΔS increases, and ΔG of the system becomes greater than 0. Hence, the entropy term dominates the enthalpy one, leading to an unfavorable Gibbs free energy state, resulting in the aggregation of hydrophobic groups that compensate for entropy loss [68]. At this point, hydrophilic NH and C=O groups are mostly embedded in the interior of the PNIPAAm molecules, and intramolecular NH··OC hydrogen bonds are formed. Moreover, the hydrophobicity of the hydrophobic isopropyl groups is enhanced, resulting in a change of the molecular chain from an extended conformation to a collapsed spherical structure. Meanwhile, long alkyl chains (i.e., HDTMS) that are hydrophobic and oleophilic are exposed outside the polymer chains, allowing the foam to adsorb oil selectively from the oil–water mixture and repel water.

3.3 Oil desorption performance of P-Fe_3O_4-PDA@MF foam

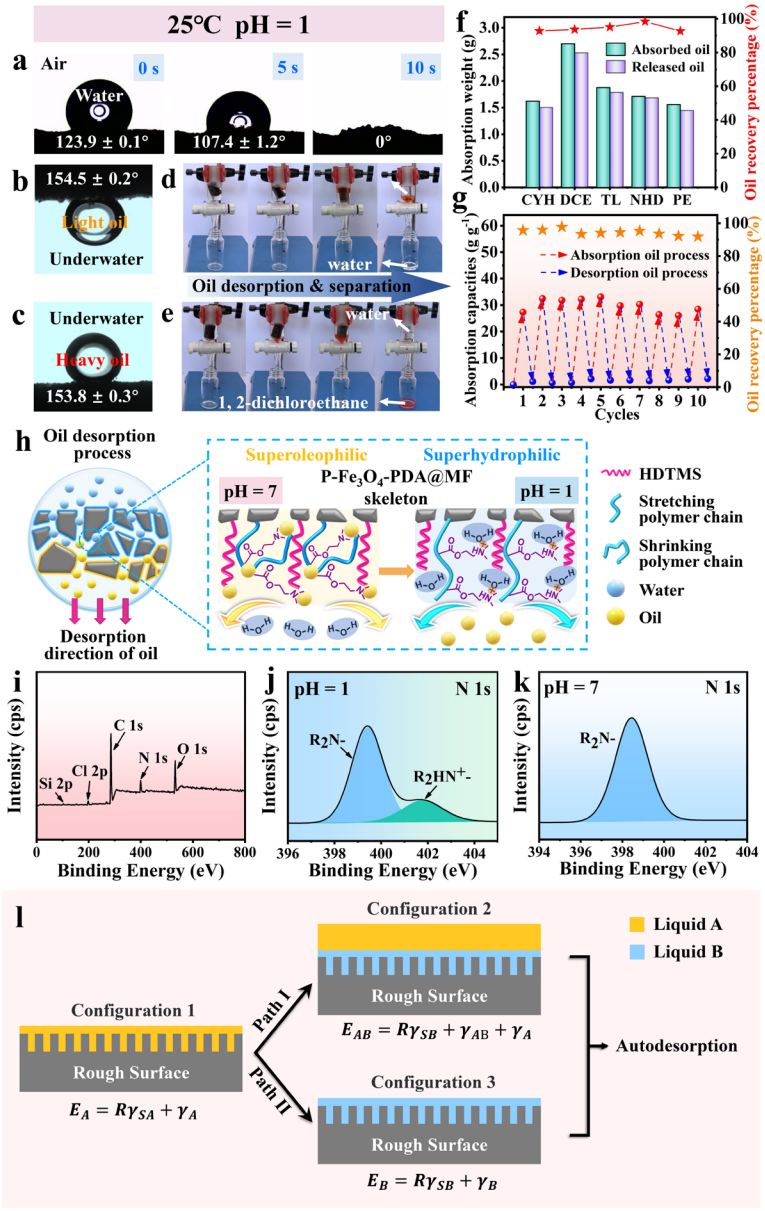

Fig. 4. a) WCAs of P-Fe_3O_4-PDA@MF at pH = 1. UWOCA diagrams of b) light oil (cyclohexane) and c) heavy oil (1, 2-dichloroethane) on the P-Fe_3O_4-PDA@MF surface. Photographs of the P-Fe_3O_4-PDA@MF desorption process of d) underwater light oil (cyclohexane) and e) heavy oil (1, 2-dichloroethane). f) Oil absorption and desorption efficiency diagram of different oily substances (CYH: cyclohexane, DCE: 1, 2-dichloroethane, TL: toluene, NHD: n-hexadecane, PE: petroleum ether). g) Cyclic oil absorption–desorption tests diagram of P-Fe_3O_4-PDA@MF. h) Mechanism diagram of oil desorption process of P-Fe_3O_4-PDA@MF. i) XPS spectrum of P-Fe_3O_4-PDA@MF at pH = 1. XPS spectra of N1s at j) pH = 1, k) pH = 7. l) Thermodynamic infused-liquid-switchable models.

Excellent desorption performance is the principle of recycling oil. The introduction of a pH-sensitive DMAEMA component allows the protonation of the prepared P-Fe_3O_4-PDA@MF to an amine salt, thereby changing the surface wettability of P-Fe_3O_4-PDA@MF foam. In the process of adjusting the pH of the foamed aqueous solution from 7 to 1, the instantaneous WCA on the P-Fe_3O_4-PDA@MF surface gradually decreases (**Fig. S5**). When pH = 1, the droplets thoroughly wet the foam after 10 s, making the foam more hydrophilic (WCA = 123.9 ± 0.1°) than under neutral conditions (**Fig. 4a**). Additionally, P-Fe_3O_4-PDA@MF foam exhibits underwater superoleophobicity with pH = 1. The OCA of the light oil (cyclohexane) and heavy oil (1,2-dichloroethane) underwater can reach 154.5 ± 0.2° and 153.8 ± 0.3° (**Fig. 4b and c**), respectively, and the foam changes from an oleophilic to a hydrophilic and an underwater superoleophobic nature. The saturated foams absorbing light oil (cyclohexane) and heavy oil (1,2-dichloroethane) were placed into a separation device filled with a small amount of water at 25°C, as shown in **Fig. 4d and e** (**Video S2**), respectively. After adjusting the pH of the aqueous solution to 1, the oil droplets were extruded gradually and automatically from the foam, and the oil-absorbing foam was regenerated. The separation and recovery of light or heavy oil from water were realized by adjusting the separation valve. The recovery rate of the autodesorption of oily substances reached up to 98.4% (**Fig. 4f**).

A test of the cyclic absorption–desorption of oil (1,2-dichloroethane) revealed that the desorption recovery rate of P-Fe_3O_4-PDA@MF foam at the 10^{th} cycle still reached 91.9% (**Fig. 4g**), indicating good recycling performance. That is, the oil can be desorbed and recovered

independently without damaging the oil absorption pore structure of the foam. The oil can be recycled without consuming energy. The pH-responsive effect of the surface molecules on foam in the desorption process of oil is explained further in the following paragraphs.

As shown in the schematic (**Fig. 4h**), when the pH of the aqueous solution is adjusted to 1, the tertiary amino groups on PDMAEMA molecular chains in the polymer are protonated under the action of acids, forming positively charged ammonium salts. These salts can easily combine with water molecules to form hydrogen bonds that increase the hydrophilicity of the foam [69]. Meanwhile, the water molecules are absorbed by hydrophilic and oleophobic polymer chains into the foam pores, which continuously extrude the oil in the foam pores to desorb the oil. The N1s XPS spectra (**Fig. 4i–k**) validate the surface changes in the PDMAEMA molecular chains under the pH response. After immersion in the solution with pH = 1, a new Cl 2p peak appears in the entire spectrum, and a strong R_2HN^+– peak (401.6 eV) appears in the N1s spectrum, suggesting that the PDMAEMA chain segment was protonated, thereby improving the hydrophilicity of the polymer chains. When the oil-absorbing foam needs to be recycled, the initial state of the foam can be restored after adjusting to pH = 7. Moreover, the R_2HN^+– peak can be transformed to the R_2N– peak (398.4 eV) of PDMAEMA, suggesting that it is deprotonated completely and restored to its original state so that the foam can be recycled.

As shown in **Fig. 4l**, before further exploring the underlying infused liquid–switchable mechanism in the process of oil autodesorption, it is first essential to define configuration 1, in which a rough solid surface is wetted preferentially by A. If liquid B replaces A, wetting the solid surface, and liquid A floats on top of B forming an AB interface, this model is defined as

configuration 2. If liquid B replaces A, wetting the solid surface, and liquid A is desorbed from B, this model is defined as configuration 3. Whether the above two assumptions can occur can be evaluated from the interfacial energy difference of the transformation paths (path I: from configuration 1 to 2, and path II: from configuration 1 to 3). For paths I and II, the interfacial energy differences can be expressed further by Eqs. (6) and (7), respectively [70-72]:

$$\Delta E_1 = R(\gamma_{SA} - \gamma_{SB}) - \gamma_{AB} \quad (6)$$

$$\Delta E_2 = R(\gamma_{SA} - \gamma_{SB}) + \gamma_A - \gamma_B \quad (7)$$

where γ_{SA} and γ_{SB} are the interfacial tensions of the liquid A–solid interface and liquid B–solid interface, respectively. γ_A and γ_B represent the surface tensions of liquids A and B, respectively. γ_{AB} represents the interfacial tensions of liquids A and B and R is the roughness factor of the solid surface. Based on Wenzel's equation (**Fig. S6**), Eqs. (6) and (7) can be further expressed as Eqs. (8) and (9) :

$$\Delta E_1 = R(\gamma_{\mathrm{B}}\cos\theta_B^* - \gamma_{\mathrm{A}}\cos\theta_A^*) - \gamma_{\mathrm{AB}} \quad (8)$$

$$\Delta E_2 = R(\gamma_{\mathrm{B}}\cos\theta_B^* - \gamma_{\mathrm{A}}\cos\theta_A^*) + \gamma_{\mathrm{A}} - \gamma_{\mathrm{B}} \quad (9)$$

where θ_A^* and θ_B^* are the apparent contact angles of liquids A and B on the solid surface, respectively. Hence, the aforementioned theoretical model was used to verify the feasibility of the desorption process of cyclohexane and 1,2-dichloroethane in the foam. Table 1 lists the measured parameters in Eqs. (8) and (9) as well as the calculated interfacial energy difference. The results suggest that when A is cyclohexane and B is an aqueous solution with pH = 1, both paths 1 and 2 exceed zero. According to the theory that the preferred wetting state has the lower surface energy [73], the process of paths 1 and 2 can occur, i.e., after the foam that absorbed cyclohexane is placed

into an aqueous solution with pH = 1, water will automatically replace cyclohexane to wet the foam, and cyclohexane will be autodesorbed from the foam. Similarly, 1,2-dichloroethane can also be desorbed from foam. The above theoretical analysis is consistent with the experimental results.

Table 1. Feasibility evaluation of the oil autodesorption process according to the interfacial energy difference.

Liquid A	Liquid B	γ_L [$\mathbf{mJ \cdot m^{-2}}$]		γ_{AB} [$\mathbf{mJ \cdot m^{-2}}$]	θ^*[°]		ΔE		Autodesorption	
		γ_A	γ_B		θ_A^*	θ_B^*	ΔE_1	ΔE_2	Theory	Exp.[a]
CYH[b]	Aqueous solution (pH = 1)	24.94	66.48	17.59	154.5	0	>0	>0	Y[d]	Y
DCE[c]	Aqueous solution (pH = 1)	30.85	66.48	42.87	153.8	0	>0	>0	Y	Y

[a]Exp.: experiment; [b]CYH: cyclohexane; [c]DCE: 1,2-dichloroethane; [d]Y represents the autodesorption process is feasible

3.4 Photothermal absorption and desorption properties of viscous crude oil

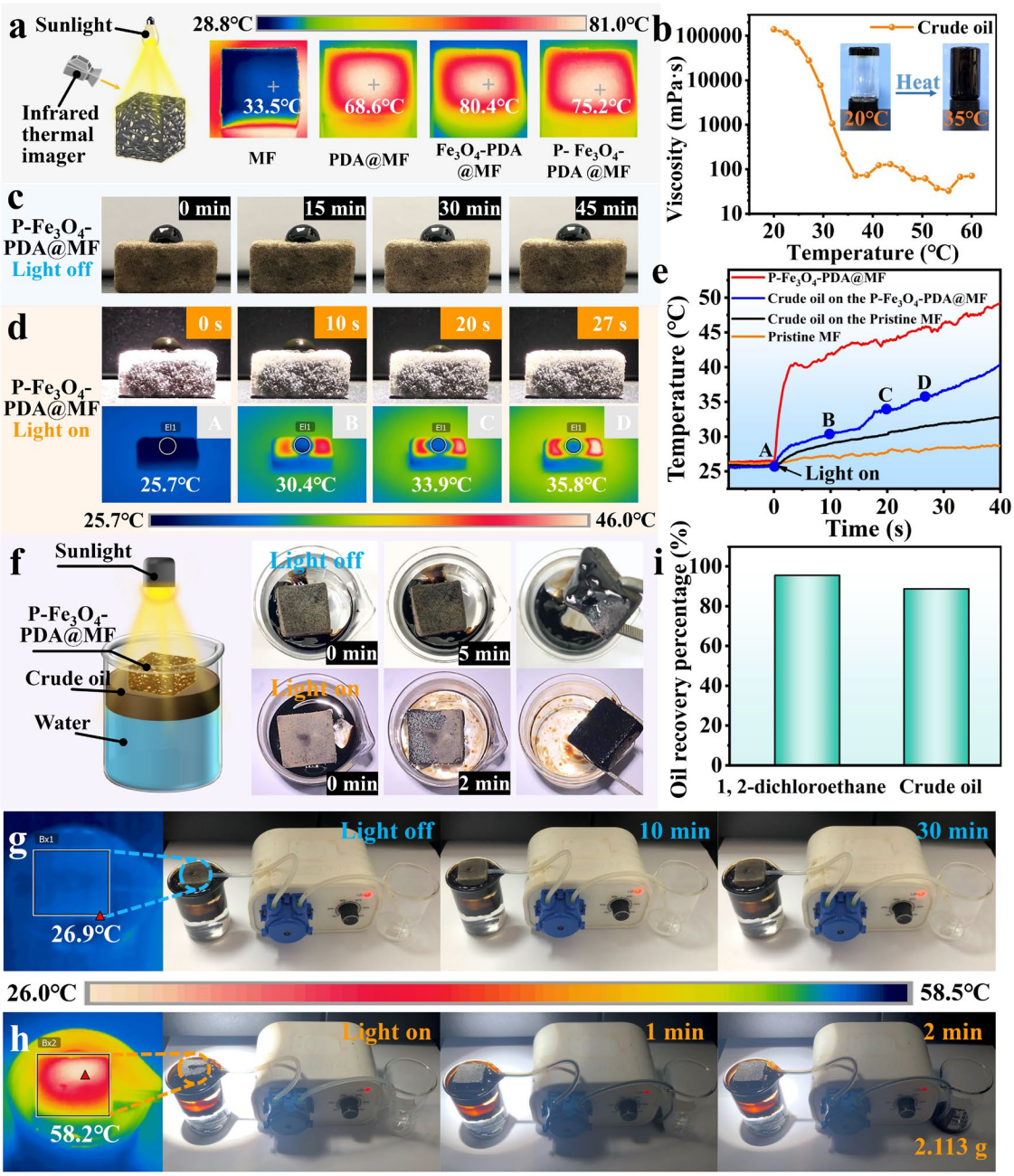

Fig. 5. a) Infrared thermal image of foams at different modification stages after illumination (1.0 kW m^{-2}). b) Viscosity of crude oil at different temperatures. c) Crude oil absorption state on the P-Fe_3O_4-PDA@MF without illumination, and d) with illumination. e) Curve of the temperature of P-Fe_3O_4-PDA@MF and pristine MF during crude oil absorption. f) Absorption process of simulated offshore crude oil on water. g) Continuous absorption process and infrared thermal image of crude oil using a peristaltic pump under no illumination or h) with illumination. i) Recovery percentage of crude oil and 1,2-dichloroethane.

The adsorption and desorption of highly viscous crude oil on the foam are difficult because of its poor fluidity, which limits its recycling. Herein, Fe_3O_4/PDA NPs with photothermal properties were introduced into the foam. A xenon lamp was used to simulate sunlight (illumination intensity: 1.0 kW m^{-2}) to irradiate foam at different stages of modification, and the light-to-heat conversion characteristic of the foam was investigated using an infrared thermal imager (**Fig. 5a**). After illumination for approximately 10 min, the upper surface temperature of the pristine foam increased from room temperature to 33.5°C; however, the temperature change was not obvious. Conversely, the surface temperature of the foam modified by PDA increased remarkably to 68.6°C and that of the Fe_3O_4-PDA@MF foam modified by the PDA/Fe_3O_4 NPs reached 80.4°C. The results suggest that PDA/Fe_3O_4 NPs as endothermic materials are key to improving the photothermal conversion efficiency.

Unlike in the case of Fe_3O_4-PDA@MF, the temperature of P-Fe_3O_4-PDA@MF (75.2°C) decreased slightly because it was coated with a polymer layer. However, it still had excellent photothermal properties and provided a thermal conductive source for reducing the viscosity of the crude oil on foam surfaces. As shown in **Fig. 5b**, the viscosity of crude oil decreased from 1.39 × 10^5 mPa s to approximately 71.77 mPa s when the temperature of the oil increased from 20°C to above 35°C, showing a clear decrease of four orders of magnitude. In glass bottles with viscous crude oil placed upside down, crude oil solidifies at the bottom at 20°C and cannot flow. When the temperature was increased to 35°C, the fluidity of the crude oil was enhanced remarkably so that the flow clung to the bottle wall, indicating that increasing the temperature can increase the fluidity of the oil. At an ambient temperature of 25°C without light, the viscous crude oil droplets remained on the surface of the P-Fe_3O_4-PDA@MF foam for 45 min without any obvious morphological changes. They could not be absorbed by the foam (**Fig. 5c**).

Under illumination (illumination intensity: 1.0 kW m^{-2}), however, P-Fe_3O_4-PDA@MF foam heated up rapidly owing to its photothermal property, as shown in **Fig. 5d**. The viscosity of the crude oil was reduced considerably within 10 s when its temperature was increased to 30.4°C, enhancing its flow penetration. Conversely, the viscosity was remarkably reduced by 27 s when the temperature of crude oil was increased to 35.8°C, and it could penetrate the oil-absorbing foam. The heating curves of the P-Fe_3O_4-PDA@MF, pristine MF, and crude oil droplets above them under illumination were recorded (**Fig. 5e**). The heating of the crude oil was attributed to the greater photothermal response of P-Fe_3O_4-PDA@MF compared to that of the pristine MF (**Fig. S7**). The rapid heating of the foam caused an increase in the temperature of crude oil by heat conduction, thereby reducing the viscosity of crude oil.

Under photothermal action, the P-Fe_3O_4-PDA@MF foam exhibits oleophilicity in air and underwater, which accelerates the absorption of heavy oil by the foam. Consequently, the capacity of this foam to absorb crude oil reaches 12.8 g g^{-1}. Additionally, the recovery experiment of the simulated spilled oil further confirmed the photothermal effect of the foam on improving the recovery rate of spilled oil. As shown in **Fig. 5f**, in the absence of light, P-Fe_3O_4-PDA@MF is placed on the surface of crude oil. After 5 min of adsorption, the crude oil only adheres to the surface of the foam and cannot penetrate the inside of the pore of the foam. However, after irradiation by a xenon lamp (illumination intensity: 1.0 kW m^{-2}) for 2 min, all the crude oil floating on the water penetrates the foam. In the experiment, 2.113 g of crude oil was recovered continuously by a peristaltic pump (**Fig. 5g and h**), and the complete recovery of the spilled oil from the water was realized.

However, foam regeneration and oil recovery are more challenging for crude oil than for low-viscosity oil. As shown in **Fig. 5i**, at 25°C, when the pH is adjusted to 1, the pH-responsive

PDMAEMA chain segment is more hydrophilic, allowing the effective desorption of the light oil (desorption rate: 95.5%) as well as exhibiting excellent desorption performance for crude oil (88.7%) (**Fig. S8**). Overall, the P-Fe_3O_4-PDA@MF foam has excellent absorption performance to viscous crude oil owing to the photothermal effect and good autodesorption recovery of crude oil because of the pH response.

3.5 Separation of oil–in–water emulsion containing bacteria and photothermal antibacterial properties

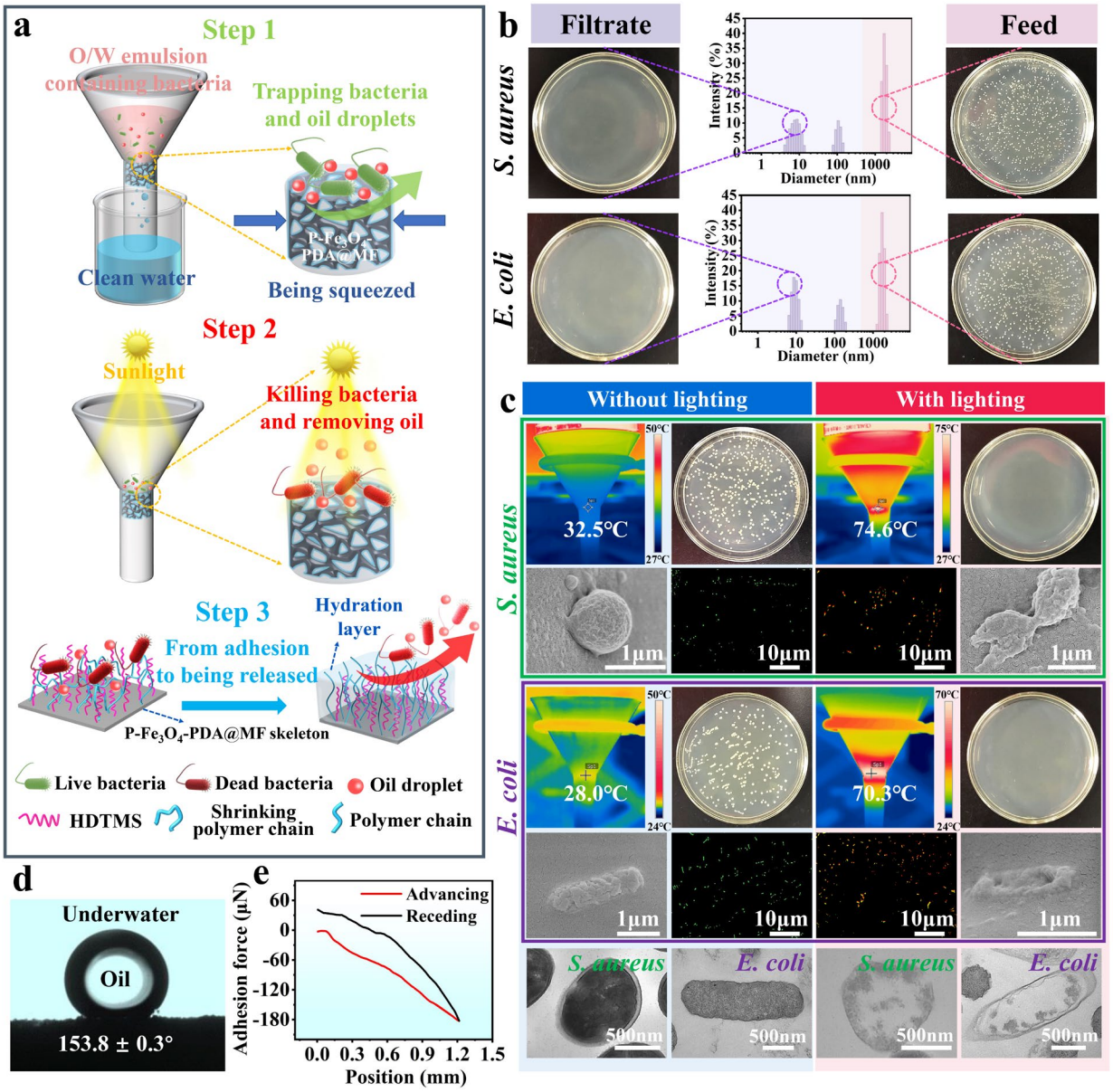

Fig. 6. a) Mechanism diagram of filtration and photothermal sterilization for bacteria-containing emulsion. b) Images and particle size distribution of an emulsion containing *S. aureus* and *E. coli* coated on agar plate before and after filtration. c) Infrared thermal image of filter device load with P-Fe3O4-PDA@MF, fluorescence microscopy, colonies on the agar plate, and micromorphology of bacteria after illumination and no illumination. d) UWOCA and e) adhesion force of oil (1,2-dichloroethane) on P-Fe3O4-PDA@MF.

The P-Fe3O4-PDA@MF foam was extruded into a separation funnel to achieve the separation of oil–in–water emulsion, and the *n*-hexane–in–water emulsion (particle size: 1,868 nm) was

separated successfully (**Fig. S9**), which made the separation of oil–in–water emulsion containing bacteria possible. As shown in **Fig. 6a**, after filtering the oil–in–water emulsion containing *S. aureus* or *E. coli*, bacteria and n-hexane oil droplets were intercepted on the foam, and clean water was collected in the filter. The mean particle sizes of oil–in–water emulsions containing the bacteria before filtrations were 2,360 (*S. aureus*) and 2,365 nm (*E. coli*), respectively. After filtration, the mean particle sizes were 100.4 (*S. aureus*) and 102.4 nm (*E. coli*), respectively (**Fig. 6b**). The bacteria-containing emulsions before and after filtration were then coated on the agar plate and cultured at 37°C for 24 h. The feed emulsion contained a large number of bacterial colonies; however, no *S. aureus* or *E. coli* were found in the filtrate (**Fig. 6b**), suggesting that most of the bacteria were intercepted by the P-Fe_3O_4-PDA@MF foam.

After filtration, heat may kill bacteria on the foam because of the photothermal properties of P-Fe_3O_4-PDA@MF under xenon lamp illumination. The increase in the temperature of the P-Fe_3O_4-PDA@MF in an aqueous solution under different illumination intensities was discussed previously (**Fig. S10**). Generally, a temperature of 37°C is necessary for bacterial growth. After irradiating with a light intensity of 3.0 kW m^{-2}, the PDA/Fe_3O_4 NPs in the foam absorb sunlight and then release energy in the form of heat. After 10 min, the foam temperature increased to approximately 50°C with a predictable bactericidal effect. Therefore, after filtration, the filter device was exposed to a xenon lamp and irradiated (light intensity: 3.0 kW m^{-2}) for 90 min. An infrared thermal imager showed that the temperature of P-Fe_3O_4-PDA@MF foam in the experimental groups containing *S. aureus* and *E. coli* increased to 74.6°C and 70.3°C, respectively. The enzymes in the cells denature when the ambient temperature of the cells is approximately

50°C, thereby inhibiting the necessary metabolic reactions of cells, damaging proteins and lipids on cell membranes, and ultimately leading to bacterial death [74].

The bactericidal ability of the P-Fe_3O_4-PDA@MF surface was evaluated by determining the bacterial count. As shown in **Fig. 6c**, without illumination, after filtering, the intercepted bacteria (both for *S. aureus* and *E. coli*) were oscillated (by oscillating the P-Fe_3O_4-PDA@MF in a PBS solution for 30 min, and the bacteria fell off from the surface). After coating and culture, many bacteria were seen on the culture medium. The cell morphology of the bacteria was intact (as per SEM and TEM), and fluorescence microscopy showed that the bacteria were alive. Conversely, under illumination, the trapped bacteria were washed off and cultured; there were no bacteria on the culture medium. The bacterial cell morphology was severely deformed (as per SEM), the cell structure was destroyed, the cell membrane was broken, and the intracellular lysates were dissolved (as per the TEM). Fluorescence microscopy showed that most of the bacteria were dead. The above phenomenon showed that the P-Fe_3O_4-PDA@MF surface has the ability of photothermal sterilization.

When the temperature of the thermosensitive polymer is above the LCST (e.g., >70°C), the oleophilic groups will adsorb the bacteria outward. When the temperature of the polymer is lower than the LCST (25°C), the hydrophilic groups outward will most likely form a hydration layer [75, 76], and the hydrophilic groups outward can effectively block the oil and bacteria, making it difficult for them to adhere on the foam. The oil-adhesion force on the foam underwater was approximately 0 N, and the UWOCA of 1,2-dichloroethane was 153.8 ± 0.3° (**Fig. 6d**), suggesting that thermoresponsive polymer foam has extremely low oil adhesion and underwater

superoleophobicity. Therefore, it is difficult for oil and bacteria to adhere to the foam surface, and it is easy to recover the oil or treat the dead bacteria. In summary, the P-Fe_3O_4-PDA@MF can separate effectively oil–in–water emulsions containing bacteria and exhibit the characteristics of photothermal sterilization, oil resistance, and bacterial antiadhesion. This highlights the potential of the foam in the treatment of bacteria-containing wastewater. Further, the foam has the potential to overcome the problem of drug resistance in the case of traditional antibacterial agents [77].

3.6 Instant fire extinguishment and fire alarm applications

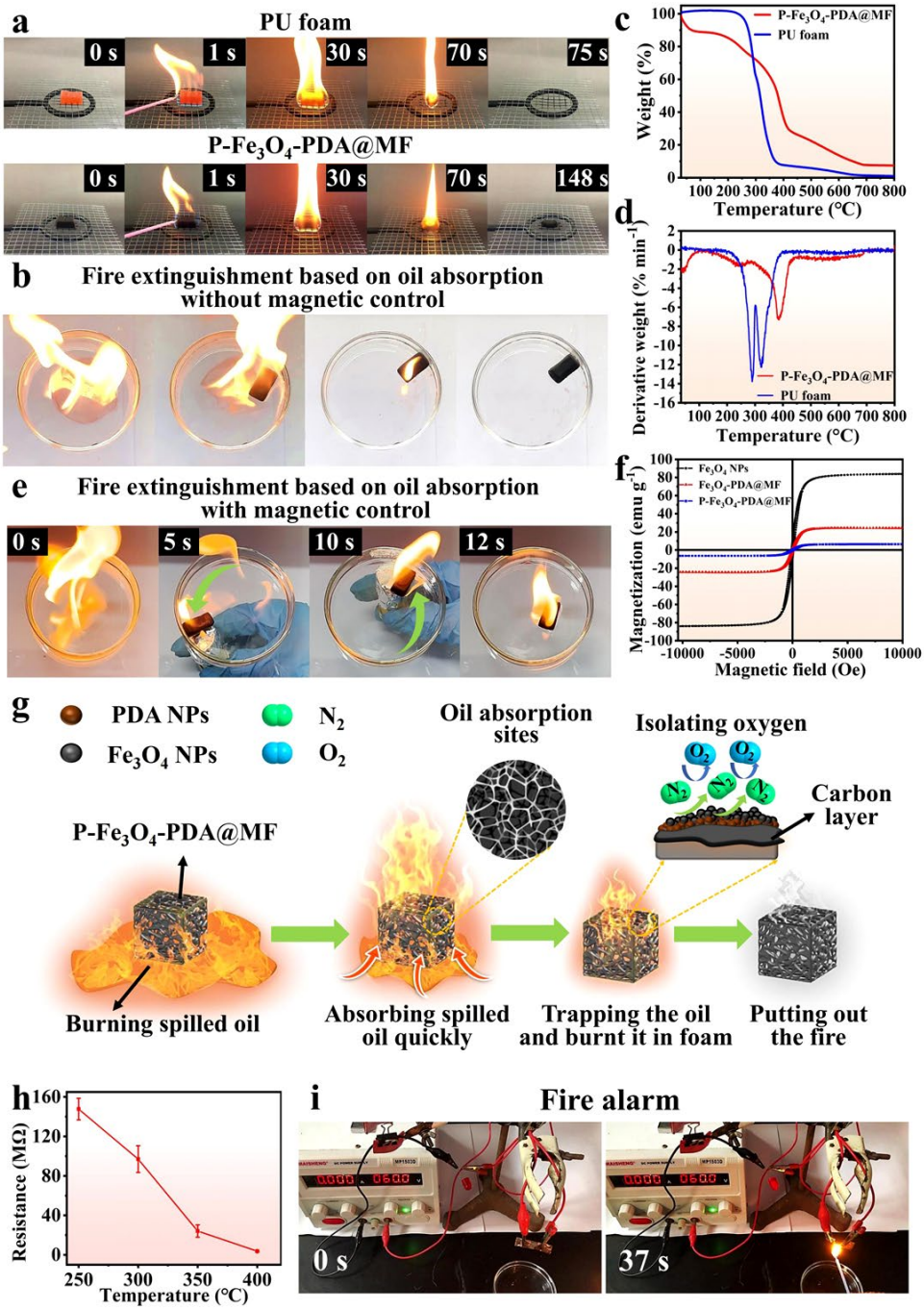

Fig. 7. a) Combustion of foam (PU and P-Fe_3O_4-PDA@MF) after oil absorption. b) Photographs of oil absorption and flame-retardancy of P-Fe_3O_4-PDA@MF. Diagrams of c) TG, d) DTG of PU foam and P-Fe_3O_4-PDA@MF. e) Photographs of magnetic oil absorption and fire extinguishing of P-Fe_3O_4-PDA@MF. f) Hysteresis loop diagram of Fe_3O_4 NPs and their modified foam. g) Mechanism diagram of oil absorption and flame-retardancy of P-Fe_3O_4-PDA@MF. h) Resistance changes of P-Fe_3O_4-PDA@MF with temperature. i) Fire alarm response of P-Fe_3O_4-PDA@MF.

Oil products are highly flammable and extremely dangerous if they catch fire. An ingenious idea is proposed herein to employ the foam to absorb oil to extinguish fire. First, the fire resistance of the foam itself was investigated. As a common commercially available oil-absorbing porous material, the PU foam burns very easily after fully absorbing cyclohexane; at 75 s after ignition, it burned to ashes without good fire resistance. Conversely, P-Fe_3O_4-PDA@MF foam can be self-extinguished at 148 s after igniting, and it retains a good foam form (**Fig. 7a**) and shows good flame retardancy. The flame-retardancy of foam materials was correlated with the thermogravimetric analysis (TGA) performance. The TGA results (**Fig. 7c and d**) showed that the initial weight loss temperature (T_0) of the PU foam was approximately 213.1°C in nitrogen. The derivative thermogravimetry (DTG) results suggest that the maximum decomposition rates of PU foam are approximately 289.4°C and 322.1°C, while the T_0 of P-Fe_3O_4-PDA@MF foam was approximately 290.5°C, and the maximum decomposition rate temperature was approximately 384.9°C; about 7.38% carbon residue remained at 800°C. The relatively outstanding flame-retarding effect and heat resistance of P-Fe_3O_4-PDA@MF foam are attributed to the addition of Fe_3O_4 NPs improving the degradation temperature of foam. These NPs hinder the volatilization of the products during polymer decomposition and act as a barrier to heat transfer. Their incorporation leads to the formation of a protective layer on the foam surface, exhibiting a certain barrier effect.

A fire extinguishing experiment was designed. After ignition and combustion of the P-Fe_3O_4-PDA@MF in a petri dish filled with spilled oil (cyclohexane), the foam was placed immediately into a petri dish. The foam absorbed the spilled oil rapidly, and the fire decreased rapidly and was eventually extinguished (**Fig. 7b**). However, the foam could only absorb the spilled oil gathered

in a small range, and it could not rapidly deal with the oil over an extensive range during the combustion processes (**Fig. S11**). Therefore, Fe_3O_4 NPs were introduced to the foam, as shown in **Fig. 7f**. The homemade Fe_3O_4 NPs showed excellent magnetic properties, with a saturated magnetization strength as high as 83.95 emu g^{-1}. The saturated magnetization strengths of Fe_3O_4-PDA@MF and P-Fe_3O_4-PDA@MF deposited by Fe_3O_4 NPs reached 24.30 emu g^{-1} and 6.40 emu g^{-1}, respectively. Although the saturated magnetization intensity decreased, the introduction of Fe_3O_4 endowed the foam with certain magnetic responsiveness. This responsiveness has potential applications in the recovery of the foam after oil–water separation or in the remote control of oil absorption.

To this end, an additional magnet was employed to manipulate the foam, and the fire-extinguishing experiment was repeated. The nonmagnetic-controlled oil absorption time was 33 s. Conversely, the magnetic-controlled foam rapidly absorbed all the oil over a wide range within only 12 s (**Fig. 7e, Video S3**). The magnetic-controlled foam rapidly reduced the temperature around the fire source and the likelihood of the fire spreading (**Fig. S12**). As shown in **Fig. S13**, when the 1,2-dichloroethane in the foam was desorbed completely, the magnetic P-Fe_3O_4-PDA@MF foam could be attracted by magnets, overcoming the interfacial tension of water, and the desorbed foam was drawn up from the water for recycling.

Additionally, the oil absorption and flame-retarding mechanism of the P-Fe_3O_4-PDA@MF foam were proposed and analyzed from the following three viewpoints. As shown in **Fig. 7g**, after placing the foam in burning spilled oil (I), the high porosity and a large number of oil-absorbing sites of P-Fe_3O_4-PDA@MF result in the rapid adsorption of the spilled oil into the foam body (II),

significantly reducing its combustion area. The thermal barrier on Fe_3O_4 NPs and the gradual formatting carbon layer on the foam surface delays the combustion process significantly and prevents the foam from collapsing during ignition. Moreover, because of the high nitrogen content of the MF, N_2 is released as a protective gas at high temperatures [78]. Hence, oxygen is isolated, and continued combustion is prevented (III). Eventually, the spilled oil is trapped in the foam until the fire is extinguished (IV). Hence, the P-Fe_3O_4-PDA@MF can be used for oil absorption for extinguishing fires, avoiding the spread and diffusion of fire, and particularly, in the inconvenient case of fire extinguishers, for which its unique advantages can be employed.

Finally, the potential applications of P-Fe_3O_4-PDA@MF in fire-sensing alarms can provide knowledge regarding a fire situation remotely to enable taking rapid emergency measures. When a fire occurs, the combustion temperature of a flame can reach from 300 °C to 500 °C [79]. In this situation, the PDA/Fe_3O_4 composite particles obtain heat from outside, and some charged free radicals may be produced. Further, under the action of an external electric field, these charged free radicals will migrate and transfer electrons, thereby reducing the resistance of the P-Fe_3O_4-PDA@MF and forming a conductive loop between two adjacent contacts. On passing electricity, the warning bulb can provide an early warning to the fire. For further investigation, the influence of temperature on the resistance of the P-Fe_3O_4-PDA@MF was investigated. The foam was heated from 250°C to 400°C on a digital heating platform, and the changes in resistance were detected using a multimeter. The resistance at both ends of foam decreased (from 147.7 MΩ to 3.75 MΩ) with an increase in temperature, and the resistance tended to decrease with increasing temperature (**Fig. 7h**). Subsequently, a 60-V power supply was added to both sides of the foam, and a small

light bulb was connected to form a series circuit. When the fire source was in the vicinity of the foam, the bulb was lit up, providing an early warning, within 37 s after the foam came in contact with the flame. The early warning makes it possible to provide a sufficient and timely response time for parties to deal with significant fire risks (**Fig. 7i, Video S4**). The above experimental results showed that the P-Fe_3O_4-PDA@MF has unique advantages in instant oil absorption for fire extinguishing and providing fire alarms.

Our results were compared with those from previous reports, which are summarized in **Table 2**. The adsorption capacities of adsorbents for different types of oily substances vary but are basically at the same level. Our work shows better recovery efficiency of oily substances (maximum desorption rate: 98.4%), especially for highly viscous crude oil (viscosity approximately 88.7%), as well as excellent recyclability for cyclic separation. Most of the reported oil/adsorbent recovery methods focus on extrusion, combustion, etc., while our work adopts the oil autodesorption method. Our method can address the more complex problems of oily wastewater, such as bacterial contamination, harsh operating conditions, and fire risks.

Table 2. Comparison of various porous sorbent materials (—, ×, and √ stand for Unknown, No, and Yes, respectively.)

Porous materials	Absorbates	Absorption Capacity [g g^{-1}]	Oil/adsorbent recovery method	Oil recovery efficiency [%]	Antibacterial	Magnetic control	Flame retardant	Fire warning	Ref.
PDMS/PDA coated sponge	Crude oil	~11	Be compressed	—	×	×	×	×	[49]
Silylated wood sponge	Silicone oil, olive oil, motor oil and organic solvents	16–41	Be compressed	~70	×	×	×	×	[50]
Fe_3O_4@OA @GO-PU[a]	Olive oil, canola oil, kerosene and organic solvents	80–150	Be compressed	>99	×	√	√	×	[80]
Fe_3O_4/HDPE[b] PU sponge	Cook oil and organic solvents	15–52	Be compressed	—	×	√	×	×	[81]
Silica/graphene oxide wide ribbon@MF	Petrol oil, tetrachloromethane	—	Be compressed	—	×	×	√	√	[79]
Tannic acid-graphene aerogel	Kerosene, liquid paraffin, maize oil, soybean oil and organic solvents	15–30	Combustion	—	√	×	√	×	[82]
MF-OTS[c]/ PNIPAAm sponge	Pump oil, peanut oil and organic solvents	35–70	Thermorespon sive desorption	—	×	×	×	×	[66]
PNIPAm/PPy@ MS	Crude oil, silicone oil, mineral oil, paraffin oil, bitumen	~32	Thermorespon sive desorption	>87	×	×	×	×	[83]

Porous polyHIPE[d] monoliths	Pump oil, edible oil, crude oil and organic solvents	6.7–18.2	pH-responsive desorption	~100	×	×	×	×	[84]
pH-responsive SiO_2@MF	Silicone oil, soybean oil and organic solvents	20–50	pH-responsive desorption	—	×	×	×	×	[85]
P-Fe_3O_4-PDA@MF	Crude oil, pump oil, silicone oil and organic solvents	12.8–43.8	pH-responsive desorption	88.7–98.4	√	√	√	√	**This work**

[a]OA: oleic acid; GO: graphene oxide; [b]HDPE: high-density polyethylene; [c]OTS: octadecyltrichlorosilane; [d]HIPE: high internal phase emulsion;

4. Conclusions

A pH/thermoresponsive flame retardant and photothermal bactericidal oil–water separation P-Fe_3O_4-PDA@MF foam was developed to meet the complex requirements of oil–water separation. The proposed foam can realize the recovery of conventional spilled oil and viscous spilled crude oil and the separation of bacteria/oil/water from a bacteria-containing oily emulsion. The foam is also capable of instant fire extinguishing by means of magnetically controlled oil absorption and can provide an early fire alarm. The PDA/Fe_3O_4 composite NPs of the P-Fe_3O_4-PDA@MF can be activated photothermally under irradiation with sunlight to change the wettability of the foam, modifying its nature from hydrophilic/oleophilic to hydrophobic/oleophilic, so that it can be applied to recover conventional oil spills. The foam exhibits excellent oil absorption on water and underwater, with an oil absorption capacity of 18.67–43.83 g g^{-1} and a maximum desorption rate of 98.4%. The excellent photothermal effect of PDA/Fe_3O_4 composite NPs causes a rapid heating of viscous oil and reduces the viscosity of the oil to enhance its fluidity. The viscosity decreases by four orders of magnitude (from 1.39 × 10^5 mPa s to 71.77 mPa s). This photothermal effect greatly enhances the recovery capacity of foam to the spilled crude oil (12.8 g g^{-1}), and the introduced PDMAEMA allows the automatic desorption of the crude oil (88.7%) from the foam under a pH response without any additional energy input. Furthermore, the separation foam enabled the separation of oil and bacteria from the complex bacteria-containing oily wastewater. The foam had excellent photothermal antibacterial performance. Further, the low oil adhesion and hydration layer imparted a remarkable antifouling effect to the foam. In particular, the high nitrogen content of the MF and Fe_3O_4 NPs imparted relatively outstanding flame retardance and magnetic control, enabling the remote control of the foam to absorb the spilled oil, allowing the rapid recovery of the spilled oil over a large range of fires, and making it possible to instantly extinguish the fire. The foam also exhibited a unique advantage from the viewpoint of fire alarm response via the connection of conductive pathways. Overall, we propose a promising design strategy of oil-spill recovery under complex operating conditions. Our method has potential applications in the recovery of viscous spilled oil and oil-

absorbing materials, purification of water contaminated with microbes, fire control, and early fire alarms.

Appendix A. Supplementary data

Supplementary data to this article can be found online.

Acknowledgements

This work is supported by the National Natural Science Foundation of China (No.22078077) and the National Science Foundation of Guangdong Province (No.2021A1515010078). The authors acknowledge the financial support of Taif University Researchers Supporting Project number (TURSP-2020/14), Taif University, Taif, Saudi Arabia

References

[1] A.T. Hoang, S. Nizetic, X.Q. Duong, L. Rowinski, X.P. Nguyen, Advanced super-hydrophobic polymer-based porous absorbents for the treatment of oil-polluted water, Chemosphere 277 (2021) 130274.

[2] W. Zheng, J. Huang, S. Li, M. Ge, L. Teng, Z. Chen, Y. Lai, Advanced materials with special wettability toward intelligent oily wastewater remediation, ACS Appl. Mater. Interfaces 13 (2021) 67-87.

[3] J. Zuo, Z. Chen, Y. Zhou, Z. Liu, C. Zhou, S. Xu, J. Cheng, X. Wen, P. Pi, Superwetting charged copper foams with long permeation channels for ultrafast emulsion separation and surfactant removal, J. Mater. Chem. A 9 (2021) 13170-13181.

[4] Z.-K. Li, Y. Liu, L. Li, Y. Wei, J. Caro, H. Wang, Ultra-thin titanium carbide (MXene) sheet membranes for high-efficient oil/water emulsions separation, J. Membr. Sci. 592 (2019) 117361.

[5] M. Elektorowicz, S. Habibi, R. Chifrina, Effect of electrical potential on the electro-demulsification of oily sludge, J. Colloid Interface Sci. 295 (2006) 535-41.

[6] J. Aurell, B.K. Gullett, Aerostat sampling of PCDD/PCDF emissions from the gulf oil spill In situ burns, Environ. Sci. Technol. 44 (2010) 9431-9437.

[7] E.B. Kujawinski, M.C. Kido Soule, D.L. Valentine, A.K. Boysen, K. Longnecker, M.C. Redmond, Fate of dispersants associated with the deepwater horizon oil spill, Environ. Sci. Technol. 45 (2011) 1298-306.

[8] S. Ye, G. Zeng, H. Wu, C. Zhang, J. Dai, J. Liang, J. Yu, X. Ren, H. Yi, M. Cheng, C. Zhang, Biological technologies for the remediation of co-contaminated soil, Crit. Rev. Biotechnol. 37 (2017) 1062-1076.

[9] Y.J. Chan, M.F. Chong, C.L. Law, D.G. Hassell, A review on anaerobic–aerobic treatment of industrial and municipal wastewater, Chem. Eng. J. 155 (2009) 1-18.

[10] M. Han, J. Zhang, W. Chu, J. Chen, G. Zhou, Research progress and prospects of marine oily wastewater treatment: a review, Water 11 (2019) 2517.

[11] V. Broje, A.A. Keller, Effect of operational parameters on the recovery rate of an oleophilic drum skimmer, J. Hazard. Mater. 148 (2007) 136-43.

[12] A. Mahringer, M. Hennemann, T. Clark, T. Bein, D.D. Medina, Energy efficient ultrahigh flux separation of oily pollutants from water with superhydrophilic nanoscale metal-organic framework architectures, Angew. Chem. Int. Ed. Engl. 60 (2021) 5519-5526.

[13] Q. Ma, H. Cheng, A.G. Fane, R. Wang, H. Zhang, Recent development of advanced materials with special wettability for selective oil/water separation, Small 12 (2016) 2186-202.

[14] B. Wang, W. Liang, Z. Guo, W. Liu, Biomimetic super-lyophobic and super-lyophilic materials applied for oil/water separation: a new strategy beyond nature, Chem. Soc. Rev. 44 (2015) 336-61.

[15] Z. Xue, Y. Cao, N. Liu, L. Feng, L. Jiang, Special wettable materials for oil/water separation, J. Mater. Chem. A 2 (2014) 2445-2460.

[16] X. Zeng, W. Cai, S. Fu, X. Lin, Q. Lu, S. Liao, H. Hu, M. Zhang, C. Zhou, X. Wen, S. Tan, A novel Janus sponge fabricated by a green strategy for simultaneous separation of oil/water emulsions and dye contaminants, J. Hazard. Mater. 424 (2022) 127543.

[17] Y.Q. Wang, W.H. Xie, H. Liu, H.B. Gu, Hyperelastic magnetic reduced graphene oxide three-dimensional framework with superb oil and organic solvent adsorption capability, Adv. Compos. Hybrid Mater. 3 (2020) 473-484.

[18] Y. Xu, G. Wang, L. Zhu, L. Shen, Z. Zhang, T. Ren, Z. Zeng, T. Chen, Q. Xue, Multifunctional superhydrophobic adsorbents by mixed-dimensional particles assembly for polymorphic and highly efficient oil-water separation, J. Hazard. Mater. 407 (2021) 124374.

[19] Q. Song, J. Zhu, X. Niu, J. Wang, G. Dong, M. Shan, B. Zhang, H. Matsuyama, Y. Zhang, Interfacial assembly of micro/nanoscale nanotube/silica achieves superhydrophobic melamine sponge for water/oil separation, Sep. Purif. Technol. 280 (2022) 119920.

[20] J. Hu, J. Zhu, S. Ge, C. Jiang, T. Guo, T. Peng, T. Huang, L. Xie, Biocompatible, hydrophobic and resilience graphene/chitosan composite aerogel for efficient oil−water separation, Surf. Coat. Technol. 385 (2020) 125361.

[21] Z. Huang, Y. Zheng, H. Zhang, F. Li, Y. Zeng, Q. Jia, J. Zhang, J. Li, S. Zhang, High-yield production of carbon nanotubes from waste polyethylene and fabrication of graphene-carbon nanotube aerogels with excellent adsorption capacity, J. Mater. Sci. Technol. 94 (2021) 90-98.

[22] Z.-H. Zhang, Z.-Y. Chen, Y.-H. Tang, Y.-T. Li, D. Ma, G.-D. Zhang, R. Boukherroub, C.-F. Cao, L.-X. Gong, P. Song, K. Cao, L.-C. Tang, Silicone/graphene oxide co-cross-linked aerogels with wide-temperature mechanical flexibility, super-hydrophobicity and flame resistance for exceptional thermal insulation and oil/water separation, J. Mater. Sci. Technol. 114 (2022) 131-142.

[23] S.-L. Li, J. Wang, H.-B. Zhao, J.-B. Cheng, A.-N. Zhang, T. Wang, M. Cao, T. Fu, Y.-Z. Wang, Ultralight Biomass Aerogels with Multifunctionality and Superelasticity Under Extreme Conditions, ACS Appl. Mater. Interfaces 13 (2021) 59231-59242.

[24] M. Cao, S.L. Li, J.B. Cheng, A.N. Zhang, Y.Z. Wang, H.B. Zhao, Fully bio-based, low fire-hazard and superelastic aerogel without hazardous cross-linkers for excellent thermal insulation and oil clean-up absorption, J. Hazard. Mater. 403 (2021) 123977.

[25] Y. Song, J. Zhou, J.-B. Fan, W. Zhai, J. Meng, S. Wang, Hydrophilic/oleophilic magnetic Janus particles for the rapid and efficient oil-water separation, Adv. Funct. Mater. 28 (2018) 1802493.

[26] Q. Zhang, R. Wu, Y. Zhou, Q. Lin, C. Fang, A novel surface-oxidized rigid carbon foam with hierarchical macro-nanoporous structure for efficient removal of malachite green and lead ion, J. Mater. Sci. Technol. 103 (2022) 15-28.

[27] P. Song, J. Cui, J. Di, D. Liu, M. Xu, B. Tang, Q. Zeng, J. Xiong, C. Wang, Q. He, L. Kang, J. Zhou, R. Duan, B. Chen, S. Guo, F. Liu, J. Shen, Z. Liu, Carbon microtube aerogel derived from kapok fiber: An efficient and recyclable sorbent for oils and organic solvents, ACS Nano 14 (2020) 595-602.

[28] H. Chen, Y. Shen, Z. He, Z. Wu, X. Xie, Facilely fabricating superhydrophobic coated-mesh materials for effective oil-water separation: Effect of mesh size towards various organic liquids, J. Mater. Sci. Technol. 51 (2020) 151-160.

[29] S. Liu, J. Lin, Q. Chen, Z. Liu, L. Gui, L. Chen, S. Huang, X. Tian, A Strategy of liquid‐grafted slippery sponges with simultaneously enhanced absorption and desorption performances for crude oil spill remediation, Macromol. Mater. Eng. 306 (2021) 2100242.

[30] C. Liu, Y. Lin, Y.F. Dong, Y.K. Wu, Y. Bao, H.X. Yan, J.Z. Ma, Fabrication and investigation on Ag nanowires/TiO_2 nanosheets/graphene hybrid nanocomposite and its water treatment performance, Adv. Compos. Hybrid Mater. 3 (2020) 402-414.

[31] C. Ruan, K. Ai, X. Li, L. Lu, A superhydrophobic sponge with excellent absorbency and flame retardancy, Angew. Chem. Int. Ed. Engl. 53 (2014) 5556-60.

[32] Z. Yin, Y. Li, T. Song, M. Bao, Y. Li, J. Lu, Y. Li, An environmentally benign approach to prepare superhydrophobic magnetic melamine sponge for effective oil/water separation, Sep. Purif. Technol. 236 (2020) 116308.

[33] W. Chao, S. Wang, Y. Li, G. Cao, Y. Zhao, X. Sun, C. Wang, S.-H. Ho, Natural sponge-like wood-derived aerogel for solar-assisted adsorption and recovery of high-viscous crude oil, Chem. Eng. J. 400 (2020) 125865.

[34] Y. Kuang, C. Chen, G. Chen, Y. Pei, G. Pastel, C. Jia, J. Song, R. Mi, B. Yang, S. Das, L. Hu, Bioinspired solar‐heated carbon absorbent for efficient cleanup of highly viscous crude oil, Adv. Funct. Mater. 29 (2019) 1900162.

[35] R. Li, G. Zhang, L. Yang, C. Zhou, Superhydrophobic polyaniline absorbent for solar-assisted adsorption of highly viscous crude oil, Sep. Purif. Technol. 276 (2021) 119372.

[36] H. Niu, J. Li, Z. Qiang, J. Ren, Versatile and cost-efficient cleanup of viscous crude oil by an elastic carbon sorbent from direct pyrolysis of a melamine foam, J. Mater. Chem. A 9 (2021) 11268-11277.

[37] Z. Wang, Y. Xu, Y. Liu, L. Shao, A novel mussel-inspired strategy toward superhydrophobic surfaces for self-driven crude oil spill cleanup, J. Mater. Chem. A 3 (2015) 12171-12178.

[38] L. Dashairya, A. Sahu, P. Saha, Stearic acid treated polypyrrole-encapsulated melamine formaldehyde superhydrophobic sponge for oil recovery, Adv. Compos. Hybrid Mater. 2 (2019) 70-82.

[39] H.G. Shi, S.L. Li, J.B. Cheng, H.B. Zhao, Y.Z. Wang, Multifunctional Photothermal Conversion Nanocoatings Toward Highly Efficient and Safe High-Viscosity Oil Cleanup Absorption, ACS Appl. Mater. Interfaces 13 (2021) 11948-11957.

[40] J. Yang, P. Xu, Y. Yao, Y. Li, B. Shi, X. Jia, H. Song, A solar-heated Janus sponge with excellent floating stability for efficient cleanup of heavy oil, Mater. Des. 195 (2020) 108979.

[41] Y. Zhu, Y. Du, J. Su, Y. Mo, S. Yu, Z. Wang, Durable superhydrophobic melamine sponge based on polybenzoxazine and Fe3O4 for oil/water separation, Sep. Purif. Technol. 275 (2021) 119130.

[42] J. Tian, Y. Yang, T. Xue, G. Chao, W. Fan, T. Liu, Highly flexible and compressible polyimide/silica aerogels with integrated double network for thermal insulation and fire-retardancy, J. Mater. Sci. Technol. 105 (2022) 194-202.

[43] H.G. Shi, H.B. Zhao, B.W. Liu, Y.Z. Wang, Multifunctional Flame-Retardant Melamine-Based Hybrid Foam for Infrared Stealth, Thermal Insulation, and Electromagnetic Interference Shielding, ACS Appl. Mater. Interfaces 13 (2021) 26505-26514.

[44] W. Zhu, W. Huang, W. Zhou, Z. Qiu, Z. Wang, H. Li, Y. Wang, J. Li, Y. Xie, Sustainable and antibacterial sandwich-like Ag-Pulp/CNF composite paper for oil/water separation, Carbohydr. Polym. 245 (2020) 116587.

[45] W. Che, Z. Xiao, Z. Wang, J. Li, H. Wang, Y. Wang, Y. Xie, Wood-based mesoporous filter decorated with silver nanoparticles for water purification, ACS Sustain. Chem. Eng. 7 (2019) 5134-5141.

[46] J. Hu, J. Lin, Y. Zhang, Z. Lin, Z. Qiao, Z. Liu, W. Yang, X. Liu, M. Dong, Z. Guo, A new anti-biofilm strategy of enabling arbitrary surfaces of materials and devices with robust bacterial anti-adhesion via a spraying modified microsphere method, J. Mater. Chem. A 7 (2019) 26039-26052.

[47] J. Lin, X. Cai, Z. Liu, N. Liu, M. Xie, B. Zhou, H. Wang, Z. Guo, Anti-liquid-interfering and bacterially antiadhesive strategy for highly stretchable and ultrasensitive strain sensors based on cassie-baxter wetting state, Adv. Funct. Mater. 30 (2020) 2000398.

[48] X. Wu, Y. Lei, S. Li, J. Huang, L. Teng, Z. Chen, Y. Lai, Photothermal and Joule heating-assisted thermal management sponge for efficient cleanup of highly viscous crude oil, J. Hazard. Mater. 403 (2021) 124090.

[49] C. Zhang, M.-B. Wu, B.-H. Wu, J. Yang, Z.-K. Xu, Solar-driven self-heating sponges for highly efficient crude oil spill remediation, J. Mater. Chem. A 6 (2018) 8880-8885.

[50] H. Guan, Z. Cheng, X. Wang, Highly compressible wood sponges with a spring-like lamellar structure as effective and reusable oil absorbents, ACS Nano 12(10) (2018) 10365-10373.

[51] H. Bi, Z. Yin, X. Cao, X. Xie, C. Tan, X. Huang, B. Chen, F. Chen, Q. Yang, X. Bu, X. Lu, L. Sun, H. Zhang, Carbon fiber aerogel made from raw cotton: a novel, efficient and recyclable sorbent for oils and organic solvents, Adv. Mater. 25 (2013) 5916-21.

[52] Y. Yang, Z. Tong, T. Ngai, C. Wang, Nitrogen-rich and fire-resistant carbon aerogels for the removal of oil contaminants from water, ACS Appl. Mater. Interfaces 6 (2014) 6351-60.

[53] X. Gui, H. Li, K. Wang, J. Wei, Y. Jia, Z. Li, L. Fan, A. Cao, H. Zhu, D. Wu, Recyclable carbon nanotube sponges for oil absorption, Acta Mater 59 (2011) 4798-4804.

[54] Y.-Q. Li, Y.A. Samad, K. Polychronopoulou, S.M. Alhassan, K. Liao, Carbon aerogel from winter melon for highly efficient and recyclable oils and organic solvents absorption, ACS Sustain. Chem. Eng. 2 (2014) 1492-1497.

[55] S. Long, Y. Feng, Y. Liu, L. Zheng, L. Gan, J. Liu, X. Zeng, M. Long, Renewable and robust biomass carbon aerogel derived from deep eutectic solvents modified cellulose nanofiber under a low carbonization temperature for oil-water separation, Sep. Purif. Technol. 254 (2021) 117577.

[56] Y. Liu, X. Wang, S. Feng, Nonflammable and magnetic sponge decorated with polydimethylsiloxane brush for multitasking and highly efficient oil–water separation, Adv. Funct. Mater. 29 (2019) 1902488.

[57] C. Zhang, Y. Li, S. Sun, M. Kalulu, Y. Wang, X. Zhou, X. Wang, Q. Du, Y. Jiang, Novel magnetic and flame-retardant superhydrophobic sponge for solar-assisted high-viscosity oil/water separation, Prog. Org. Coat. 139 (2020) 105369.

[58] Y. Wang, Z. Liu, X. Wei, K. Liu, J. Wang, J. Hu, J. Lin, An integrated strategy for achieving oil-in-water separation, removal, and anti-oil/dye/bacteria-fouling, Chem. Eng. J. 413 (2021) 127493.

[59] X. Wu, S. Cao, D. Ghim, Q. Jiang, S. Singamaneni, Y.-S. Jun, A thermally engineered polydopamine and bacterial nanocellulose bilayer membrane for photothermal membrane distillation with bactericidal capability, Nano Energy 79 (2021) 105353.

[60] E. Zhou, D. Qiao, Y. Yang, D. Xu, Y. Lu, J. Wang, J.A. Smith, H. Li, H. Zhao, P.K. Liaw, F. Wang, A novel Cu-bearing high-entropy alloy with significant antibacterial behavior against corrosive marine biofilms, J. Mater. Sci. Technol. 46 (2020) 201-210.

[61] Xu, Hou, Smart gating multi-scale pore/channel-based membranes, Adv. Mater. 28 (2016) 7049-7064.

[62] J. Lin, X.Y. Chen, C.Y. Chen, J.T. Hu, Z. Guo, Durably antibacterial and bacterially anti-adhesive cotton fabrics coated by cationic fluorinated polymers, ACS Appl. Mater. Interfaces 10 (2018) 6124-6136.

[63] C. Zhang, Y. Ou, W.-X. Lei, L.-S. Wan, J. Ji, Z.-K. Xu, $CuSO_4/H_2O_2$-induced rapid deposition of polydopamine coatings with high uniformity and enhanced stability, Angew. Chem. Int. Ed. 55 (2016) 3054-3057.

[64] P. Yi, H. Hu, W. Sui, H. Zhang, Y. Lin, G. Li, Thermoresponsive polyurethane sponges with temperature-controlled superwettability for oil/water separation, ACS Appl. Polym. Mater. 2 (2020) 1764-1772.

[65] J. Lin, J. Hu, W. Wang, K. Liu, C. Zhou, Z. Liu, S. Kong, S. Lin, Y. Deng, Z. Guo, Thermo and light-responsive strategies of smart titanium-containing composite material surface for enhancing bacterially anti-adhesive property, Chem. Eng. J. 407 (2020) 125783.

[66] Z. Lei, G. Zhang, Y. Deng, C. Wang, Thermoresponsive melamine sponges with switchable wettability by interface-initiated atom transfer radical polymerization for oil/water separation, ACS Appl. Mater. Interfaces 9 (2017) 8967-8974.

[67] R. Hoogenboom, Chapter 2 - Temperature-responsive polymers: properties, synthesis, and applications, in: M.R. Aguilar, J. San Román (Eds.), Smart Polymers and their Applications (Second Edition), Woodhead Publishing, UK, 2019, pp. 13-44.

[68] K. Shiraga, H. Naito, T. Suzuki, N. Kondo, Y. Ogawa, Hydration and hydrogen bond network of water during the coil-to-globule transition in poly(N-isopropylacrylamide) aqueous solution at cloud point temperature, J. Phys. Chem. B 119 (2015) 5576-87.

[69] Z. Dang, L. Liu, Y. Li, Y. Xiang, G. Guo, In situ and ex situ pH-responsive coatings with switchable wettability for controllable oil/water separation, ACS Appl. Mater. Interfaces 8 (2016) 31281-31288.

[70] Q. Wang, Y. Wang, B. Wang, Z. Liang, J. Di, J. Yu, Under-liquid dual superlyophobic nanofibrous polymer membranes achieved by coating thin-film composites: a design principle, Chem Sci 10 (2019) 6382-6389.

[71] Y. Wang, J. Di, L. Wang, X. Li, N. Wang, B. Wang, Y. Tian, L. Jiang, J. Yu, Infused-liquid-switchable porous nanofibrous membranes for multiphase liquid separation, Nat Commun 8 (2017) 575.

[72] Z. Zhao, Y. Ning, X. Jin, S. Ben, J. Zha, B. Su, D. Tian, K. Liu, L. Jiang, Molecular-structure-induced under-liquid dual superlyophobic surfaces, ACS Nano 14 (2020) 14869–14877.

[73] X. Tian, V. Jokinen, J. Li, J. Sainio, R.H. Ras, Unusual dual superlyophobic surfaces in oil-water systems: The design principles, Adv. Mater. 28 (2016) 10652-10658.

[74] M.C. Wu, A.R. Deokar, J.H. Liao, P.Y. Shih, Y.C. Ling, Graphene-based photothermal agent for rapid and effective killing of bacteria, Acs Nano 7 (2013) 1281-1290.

[75] T. Wei, Z. Tang, Q. Yu, H. Chen, Smart antibacterial surfaces with switchable bacteria-killing and bacteria-releasing capabilities, ACS Appl. Mater. Interfaces 9 (2017) 37511-37523.

[76] Y. Wang, T. Wei, Y. Qu, Y. Zhou, Y. Zheng, C. Huang, Y. Zhang, Q. Yu, H. Chen, Smart, photothermally activated, antibacterial surfaces with thermally triggered bacteria-releasing properties, ACS Appl. Mater. Interfaces 12 (2020) 21283-21291.

[77] J. Lin, Y. Wang, X. Wei, S. Kong, Z. Guo, Controllable antibacterial and bacterially anti-adhesive surface fabricated by a bio-inspired beetle-like macromolecule, Int. J. Biol. Macromol. 157 (2020) 553-560.

[78] Y. Xiang, Y. Pang, X. Jiang, J. Huang, F. Xi, J. Liu, One-step fabrication of novel superhydrophobic and superoleophilic sponge with outstanding absorbency and flame-retardancy for the selective removal of oily organic solvent from water, Appl. Surf. Sci. 428 (2018) 338-347.

[79] M. Mao, H. Xu, K.-Y. Guo, J.-W. Zhang, Q.-Q. Xia, G.-D. Zhang, L. Zhao, J.-F. Gao, L.-C. Tang, Mechanically flexible, super-hydrophobic and flame-retardant hybrid nano-silica/graphene oxide wide ribbon decorated sponges for efficient oil/water separation and fire warning response, Compos. Pt. A-Appl. Sci. Manuf. 140 (2021) 106191.

[80] M. khalilifard, S. Javadian, Magnetic superhydrophobic polyurethane sponge loaded with Fe_3O_4@oleic acid@graphene oxide as high performance adsorbent oil from water, Chem. Eng. J. 408 (2021) 127369.

[81] T. Yu, F. Halouane, D. Mathias, A. Barras, Z. Wang, A. Lv, S. Lu, W. Xu, D. Meziane, N. Tiercelin, S. Szunerits, R. Boukherroub, Preparation of magnetic, superhydrophobic/superoleophilic polyurethane sponge: Separation of oil/water mixture and demulsification, Chem. Eng. J. 384 (2020) 123339.

[82] J. Luo, J. Lai, N. Zhang, Y. Liu, R. Liu, X. Liu, Tannic acid induced self-assembly of three-dimensional graphene with good adsorption and antibacterial properties, ACS Sustain. Chem. Eng. 4 (2016) 1404-1413.

[83] M. Wu, Y. Shi, J. Chang, R. Li, C. Ong, P. Wang, Sunlight induced rapid oil absorption and passive room-temperature release: An effective solution toward heavy oil spill cleanup, Adv. Mater. Interfaces 5 (2018) 1800412.

[84] Z. Guo, H. Gu, Q. Chen, Z. He, W. Xu, J. Zhang, Y. Liu, L. Xiong, L. Zheng, Y. Feng, Macroporous monoliths with pH-induced switchable wettability for recyclable oil separation and recovery, J. Colloid Interface Sci. 534 (2019) 183-194.

[85] L. Tang, G. Wang, Z. Zeng, L. Shen, L. Zhu, Y. Zhang, Q. Xue, Three-dimensional adsorbent with pH induced superhydrophobic and superhydrophilic transformation for oil recycle and adsorbent regeneration, J. Colloid Interface Sci. 575 (2020) 231-244.